VTT PUBLICATIONS 314

The effect of specimen and flaw dimensions on fracture toughness

Markku J. Nevalainen

VTT Manufacturing Technology

Dissertation for the degree of Doctor of Technology
to be presented with due permission for public examination and debate
in Auditorium K 216 at Helsinki University of Technology (Espoo, Finland)
on the 1st of July, 1997, at 12 o'clock noon

TECHNICAL RESEARCH CENTRE OF FINLAND
ESPOO 1997

ISBN 951-38-5064-1
ISSN 1235-0621

JULKAISIJA – UTGIVARE – PUBLISHER

Valtion teknillinen tutkimuskeskus (VTT), Vuorimiehentie 5, PL 2000, 02044 VTT
puh. vaihde (90) 4561, telekopio 456 4374

Statens tekniska forskningscentral (VTT), Bergsmansvägen 5, PB 2000, 02044 VTT
tel. växel (90) 4561, telefax 456 4374

Technical Research Centre of Finland (VTT), Vuorimiehentie 5, P.O.Box 2000, FIN–02044 VTT, Finland
phone internat. + 358 0 4561, telefax + 358 0 456 4374

VTT Valmistustekniikka, Ydinvoimalaitosten materiaalitekniikka, Kemistintie 3, PL 1704, 02044 VTT
puh. vaihde (09) 4561, faksi (09) 456 7002

VTT Tillverkningsteknik, Material och strukturell integritet, Kemistvägen 3, PB 1704, 02044 VTT
tel. växel (09) 4561, fax (09) 456 7002

VTT Manufacturing Technology, Materials and Structural Integrity, Kemistintie 3, P.O.Box 1704,
FIN–02044 VTT, Finland
phone international + 358 9 4561, fax + 358 9 456 7002

Technical editing Leena Ukskoski

VTT OFFSETPAINO, ESPOO 1997

Nevalainen, Markku J. The effect of specimen and flaw dimensions on fracture toughness. Espoo 1997, Technical Research Centre of Finland, VTT Publications 314. 60 p. + app. 98 p.

UCD **593.42**

Keywords **fractures (materials), cracking (fracturing), fracture tests, fracture strength, finite element analysis, flaw inspection**

ABSTRACT

Fracture toughness values obtained from standardized tests, with strict specimen size requirements to produce specimen size independent results, are used in the process of fracture toughness assessment of structural components. Often results from the standardized tests can not be applied to real flaws due to different flaw geometries in test specimen and structure or the properties of the examined material are such that strict specimen size requirements of the standards are in practise impossible to fulfill. In both cases the main cause to problems arises from combined constraint characteristics of the flaw and specimen type.

In this study a wide range of specimen and flaw dimensions were examined both by experimental tests and computational finite element analysis for constraint assessment. The methods for taking into account specimen and flaw dimensions are introduced and applied to investigated configurations. These methods include constraint correction or indexing methods, namely T-stress, Q-parameter and small-scale yielding correction (SSYC) and statistical treatment for specimen size effect in case of cleavage fracture. Experimentally studied configurations were Charpy-size impact specimens with a/W ranging from 0.05 to 0.5, static 3-point-bend (3PB) specimens with thickness ranging from 5 to 300 mm and plates in 4-point-bending (4PB) with elliptical surface cracks on the tension side. All flaws were fatigue precracked. Computationally analysed configurations included 3-dimensional surface-edge notched 3PB specimens (SE(B)) with deep (a/W = 0.5) and shallow (a/W = 0.1) crack configurations and compact tension (CT) specimens with a/W = 0.6. The W/B ratios for SE(B) and CT specimens were 1, 2 and 4. The W/B = 2 configuration was also analysed as side grooved. The strain hardening exponent (n) of the deformation plasticity material model had values 5, 10 and 20. Computationally analysed were also two sizes of elliptical surface cracks in a 4PB plate with material strain hardening exponent n = 10. For the 4PB plates a formula for fracture toughness (J_c) calculation was proposed.

The conducted 3-dimensional finite element analyses of the cracked configurations were more detailed than any analysis in previously published literature. Thus analyses revealed a great deal of new information of the in-plane constraint behaviour inside the specimen. Toughness scaling models (= SSYC) and J-Q trajectories were created and their evolution as functions of specimen dimensions, material hardening properties and applied loading were investigated.

The SSYC and J-Q approach were found to describe constraint properties adequately. This finding received partial verification from the experimental tests, where SSYC was found to be superior in comparison to Q-parameter and T-stress. The statistical treatment for specimen thickness description was very promising and a development for that method was proposed.

Based on the results, the differences in apparent fracture toughness values obtained from various different specimen configurations can be better understood and taken into account.

PREFACE

This research was in majority conducted at the VTT Manufacturing Technology within the Finnish Research Programme on the Structural Integrity of Nuclear Power Plants. The funding to the work at VTT was provided by the Ministry of Trade and Industry (KTM) and VTT Manufacturing Technology. The computational investigations were conducted at the University of Illinois in USA during year 1994. The work in USA was supported by grants principally from the U.S. Nuclear Regulatory Commission and the Naval Surface Warfare Center - Annapolis Detachment (Code 614). Support was also received from VTT Manufacturing Technology, The Finnish Academy, Foundations of Imatran Voima, W. Ahlström and Ella and Georg Ehrnrooth.

The thesis work was directed by Professor Hannu Hänninen in the Helsinki University of Technology, to whom I would like to express my gratitude for his valuable comments and advices.

I would like to thank the preliminary examiners, Professor Mauri Määttänen, the Helsinki University of Technology and Rector Aki Valkonen, the Helsinki Business Polytechnic, for their comments and remarks.

Research Professor Kim Wallin and group leader Jussi Solin I would like to thank for their encouragement, support and technical advice during the work. The group members, Merja Asikainen, Kari Santaoja, Tapio Planman, Arja Saarenheimo and Heikki Keinänen I would like to thank for their advices and guidance. I would like to express my respect and gratitude to Professor Heikki Kleemola, Research Director of the VTT Manufacturing Technology and Doctor Rauno Rintamaa, Head of the Materials and Structural Integrity Research, for their support to the work.

To Professor Robert H. Dodds, Jr., Kyle Koppenhoefer, Arne Gullerud and Parvis Banan at the University of Illinois at Urbana-Champaign I am in great debt of gratitude for their guidance in the jungle of computational analysis, bugs and viruses.

Specially, I would like to thank Arto Nyholm, Esa Varis, Heikki Laukkanen and Ensio Hosio for their help during the experimental part of the work. Sirpa Laine-Leimu, Åsa Åvall, Hilkka Hänninen and Tuomo Hokkanen I would like to thank for valuable assistance during the editing of the manuscript.

In Espoo, June 1997 *Markku J. Nevalainen*

NOMENCLATURE

σ_{ij}	stress field
A_{ij}, B_{ij}, C_{ij}	constant matrices
r, R	distance from the crack tip (polar coordinate)
θ	angle from the crack plane (polar coordinate)
K, K_c, K_{Ic}	stress intensity factor
f_{ij}, g_{ij}, h_i	matrices of functions
ε_{ij}	strain field
n	strain hardening exponent
S_{ij}	stress tensor
E_{ij}	strain tensor
J, J_c, J_{ic}	J-integral
Γ	integration path around the crack tip in the calculation of J-integral
W	strain energy density
T	traction vector in Rice's J-integral (not to be confused with T-stress)
u	displacement vector
ds	an element of arc length along Γ
Π	potential energy
T, T^e, T_i, T_{ii}	T-stress or its components
t', B, β	biaxiality coefficient
$\sigma_{\theta\theta}$	hoop stress
σ_0, σ_y	yield strength
a_i, η, m, M	coefficients
δ_{ij}	Kronecker delta

Q	Q-parameter
u_i	displacement field
ε_0, ε_{pl}	yield strain, plastic strain
α, I_n	material constant
F, G, h	functions
σ, σ_c, σ_f	(critical fracture) stress
CTOD, δ, δ_c	(critical) crack tip opening
A	area
ϕ	constraint factor
B	thickness of the through-thickness crack specimen (not to be confused with biaxiality coefficient)
b	ligament length of the through-thickness crack specimen
W	specimen width
a	crack length
P, P_f	probability
σ_w	Weibull stress (Weibull, 1939)
e	base of the natural logarithm (= 2.71828...)
P, P_L	applied load, limit load (not to be confused with probability)
U, U_{pl}	energy, plastic energy
σ_{flow}	flow stress
V	volume
$\overline{\sigma}_c$	principal stress contour
E, E’	Young’s modulus (≈ 210 GPa in plane strain and ≈231 GPa in plane stress for steel)
Mom	applied moment
t	plate thickness
2b	total plate width

c	half length of the surface crack on the plate surface
SSY(C)	Small-Scale Yielding (Correction)
FEM	Finite-Element Method
FE(A)	Finite-Element (Analysis)

CONTENTS

Appendices of this publication are not included in the PDF version. Please order the printed version to get the complete publication (http://www.inf.vtt.fi/pdf/publications/1997/)

ORIGINAL FEATURES

The following features of this thesis are believed to be original:

1. Very detailed 3-dimensional finite element analyses of SE(B) and CT specimens were conducted. The author is unaware of any previous research where this much refined mesh was used for 3-dimensional crack tip modelling. The determination of the in-plane scaling models and J-Q trajectories as functions of specimen thickness coordinate with current accuracy is unique. A refinement for the statistical treatment of fracture toughness data was derived.

2. Similarly detailed analyses of elliptical surface cracks were conducted and similar in-plane constraint parameters were derived. The mesh refinement together with the accuracy of the calculation procedures in the post-processing programs provided in-plane information of elliptical crack behaviour in a unique way. This enabled 3-dimensional comparison between in reality existing surface flaws with flaw geometries in standardized specimens.

3. Together with the computational analyses of surface cracks, a set of experimental tests were conducted. These analyses both established and to some extent verified a formula for the calculation of fracture toughness of a surface flawed plate under bending loading.

4. An extensive set of tests with a wide range of specimen configurations and loadings was performed in order to study different specimen and flaw behaviour and to investigate methods for recognizing specimen size effects in the test results.

DISSERTATION

This dissertation consists of an introductory report and four appended publications (Appendices I - IV):

Publication 1 — Nevalainen, M. & Dodds, R. H. 1996. Numerical investigation of 3-d constraint effects on brittle fracture in SE(B) and C(T) specimens. International Journal of Fracture, Vol. 74, No. 2, pp. 131 - 161.

Publication 2 — Nevalainen, M. 1997. Fracture toughness comparison between a semielliptical surface crack in a 4PB plate and a through thickness crack in a 3PB fracture toughness test specimen. Espoo: Technical Research Centre of Finland. 34 p. (VTT Publications 303.)

Publication 3 — Nevalainen, M., Wallin, K. & Rintamaa, R. 1994. Crack depth effects measured by dynamic fracture toughness tests. In: Fracture Mechanics. 24th Vol. ASTM STP 1207, John D. Landes, Donald E. McCabe and J. A. M. Boulet (eds.). American Society for Testing and Materials, Philadelphia, PA. Pp. 108 - 130.

Publication 4 — Nevalainen, M. & Wallin, K. 1994. The effect of crack depth and absolute thickness on fracture toughness of 3PB specimens. In: ECF 10 – Structural Integrity: Experiments, Models and Applications, Vol. II. K.-H. Schwalbe and C. Berger (eds.). London: European Structural Integrity Society. Pp. 997 - 1006.

1 INTRODUCTION

1.1 PROBLEM DESCRIPTION

The topic of this thesis is related to fracture mechanics, which is a branch of science dealing with micromechanics and strength of materials. Fracture mechanics is applied in order to calculate the fracture toughness of a cracked component or specimen, creating a singular stress field at the tip of the crack. Fracture toughness describes the ability to resist fracture and is dependent on component geometry, loading and material properties at the operational conditions.

In practice, steel components are in many cases too large and too expensive to be tested as such in their operating conditions for their fracture characteristics. Thus, it is more beneficial to divide the fracture toughness determination in two stages: firstly, the determination of the fracture toughness of the material as a functon of the test temperature and perhaps other operating conditions and secondly, application of a geometry dependent factor to obtain the fracture toughness of the component or its weakest part.

Specimens that can be tested in laboratories and are inexpensive enough to be broken in large numbers are used for the first stage of the fracture toughness determination. Currently, there exist numerous standards for the fracture toughness testing of metallic materials. Common to all standards is a requirement of large enough specimen size in order to obtain test results dependent solely on material properties, not on the geometry or the size of the specimen. The minimum size requirement is usually expressed as the ratio of the fracture toughness to the yield strength, multiplied by some constant, $M \cdot J_C/\sigma_Y$. The reason for this size requirement is to maintain a large elastically behaving material volume around the plastically behaving region near the specimen crack tip. This condition is generally referred to as small scale yielding (SSY) in comparison to the unwanted large scale yielding (LSY). Under large scale yielding the specimen boundaries affect the crack tip stress field by relaxing the triaxial stress state and increasing the apparent fracture toughness. This phenomenon is referred to as the constraint effect.

Problems are encountered with the size requirement. Usually low strength materials have high fracture toughness and so the minimum required specimen size for those materials may be very large, in some cases of the order of several meters. This leads to the need of larger testing machines which increases costs. On the other hand, in some cases the specimen size is limited due to manufacturing process or material availability. For example, irradiated specimens must be small due to limited volume of the irradiation chambers and strong neutron flux gradients. Thus, the maximum irradiated specimen size becomes far smaller than required by the standards. Due to the above mentioned reasons, testing of

standardized specimens is in some cases uneconomical or impossible and smaller specimens have to be tested to get an idea of the fracture toughness level. This results in a problem of obtaining a geometry independent result from the test results obtained with too small specimens, i.e. the removal of the geometry effect.

In real operating components and structures the flaws are seldom straight through thickness cracks as in standardized test specimens. Often real cracks are long and shallow, beginning and ending at one surface of the structure. A pressure vessel is a typical structure with this kind of flaw geometry. This brings another difficulty into fracture toughness estimation. Not only the geometry of the component, but also the geometry and size of the flaw affect the fracture toughness determination. For shallow cracks the constraint effect increases the apparent fracture toughness very much due to the short distance from the crack tip to the free surface.

There are two, parallel ways to investigate the geometry effect on fracture toughness: experimental and computational analysis, the latter referring often to Finite Element Method (FEM). This thesis includes both types of approaches. Experimental fracture toughness values have been determined for specimens with either varying thickness (B), varying ratio of crack depth to specimen width (a/W) or varying flaw geometry from through thickness to elliptical surface cracks. Extensive finite element analyses (FEA) have been applied for models with geometries ranging from standardized specimens to plates with surface flaws, having specimen thickness, crack size and material strain hardening exponent as parameters. Also effects of side grooving have been studied.

Three types of approaches have been applied to find out the constraint correction for different geometries, namely T-stress, Q-parameter and small-scale yielding correction (SSYC). Also statistical treatment for specimen thickness effect in case of cleavage fracture was investigated. The approaches were applied both for experimental and computational results.

1.2 PRESENT STATUS OF FRACTURE MECHANICS

One milestone of fracture mechanics was the introduction of the J-integral in the late 1960's (Rice, 1968). No later than 1973 Larsson & Carlsson presented first arguments about the effect of specimen geometry on the value of the calculated J-integral. The issue was then acknowledged (for example Rice, 1974), but did not cause significant discussion, if measured as the number of related published articles. During the 70's and 80's the topics of constraint effect and correlations between small and large specimen results were studied quite actively, for example within the American Society for Testing and Materials: Special Technical Publication (ASTM STP) series, but the T-term remained approximately two decades as the only parameter for constraint description. The introduction of the Q-parameter (O'Dowd & Shih, 1991 and 1992) and the SSY-correction (Dodds et al., 1991) finally expanded the on-going discussion of the constraint effect.

Several empirically and computationally oriented articles concerning the effect of specimen thickness and ratio of crack depth to specimen width (a/W) on measured fracture toughness have been published during last ten years. Most of the empirical analyses have involved correlations between small and large specimen fracture toughness results in the ductile-to-brittle transition region. Some examples are the Heavy Section Steel Technology Program (HSST) sponsored by Nuclear Regulatory Commission (NRC) (Theiss et al., 1994) and the international program initiated by Japan Society for the Promotion of Science (JSPS) and Materials Properties Council (MPC) including participants from Asia, America and Europe (Iwadate & Yokobori, 1994 and Van Der Sluys & Miglin, 1994). Computational analyses have mostly described specimen boundary effects on the near crack-tip stress distribution.

The first significant review of the status of research being conducted on surface cracks was the American Society of Mechanical Engineers (ASME) symposium ”The Surface Crack: Physical Problems and Computational Solutions” in 1972 (Reuter et al., 1990). In 1986 ASTM and Society for Experimental Mechanics (SEM) initiated a joint effort to identify the international state-of-the-art of research on surface flaws, which resulted in two symposia. Papers of analytical, numerical and experimental analyses were presented, but the majority of presentations dealt with elastic stress intensity factor determination, while research on nonlinear behaviour was very limited. One evident explanation for this is the need to predict surface crack growth under fatigue loading.

With the increased accessability of powerful (super)computers the interest to model 3-dimensional specimens (and components) with surface cracks has grown. Active reaseach has been focused on the development of stress states inside a standardized specimen and evolution of crack-tip constraint conditions along a curved crack front. Cracking of bimaterial interfaces, subclad cracking, multiple parallel cracks in a component and development of the weight function method for stress intensity factor calculation for arbitrary shaped crack fronts are among the other areas of active reasearch.

2 CRACK TIP CHARACTERIZATION

The characterization of the crack-tip stress and strain fields is fundamental in fracture mechanics, since the crack tip fields and perhaps their interference with the boundary effects determine the fracture process. In the following some significant publications during the development of fracture toughness analysis are referenced.

Williams (1957) presented a serie expansion of the crack tip stress field, Eq. 1.

$$\sigma_{ij} = A_{ij}(\theta) r^{-1/2} + B_{ij}(\theta) + C_{ij}(\theta) r^{1/2} + \ldots, \tag{1}$$

where r and θ are the polar coordinates at the crack tip. The first term in the expansion is singular and the most dominant term close to the crack tip, where r $\rightarrow$ 0. The second term is independent of the r coordinate and the rest of the terms are positive powers of the r and thus have very little effect on the crack tip stress field.

The basis of fracture mechanics is the elastic analysis of the crack tip region which shows a unique stress-strain field with a singularity at the crack tip. The strength of the crack tip singularity is the stress intensity factor K, Eq. 2. The crack tip region can then be characterized by one parameter and fracture is assumed to occur for some critical value of K (K_c).

$$\sigma_{ij} = \frac{K}{\sqrt{2\pi r}} f_{ij}(\theta) \tag{2}$$

For example, the ASTM standard for plane strain fracture toughness determination (ASTM, 1996) uses the stress intensity factor for fracture toughness determination provided that the plastic zone near the crack tip is very small compared to other dimensions of the test specimen.

A direct extension of fracture mechanics concepts to cases of large scale yielding would assume again the existence of crack tip singularity. Hutchinson (1968) and Rice & Rosengren (1968) (referred to as HRR) proved that a singularity does exist which is uniquely dependent on the material flow properties. In solved cases of crack tip fields, they suggested dependence of stress and strain fields on distance r from the crack tip and on strain hardening exponent n, Eqs. 3.

$$\begin{aligned} s_{ij} &\propto r^{-n/(1+n)} S_{ij}(q) \\ e_{ij} &\propto r^{-1/(1+n)} E_{ij}(q) \end{aligned} \tag{3}$$

Rice (1968) proposed existence of a path-independent J-integral, Eq. 4.

$$J = \int_{\Gamma} \left(W dy - T \cdot \frac{\partial u}{\partial x} ds \right) \tag{4}$$

J-integral characterizes the crack tip area without focusing attention directly at the crack tip, which provides a more practical method for analysing fracture. The value of the J-integral depends on the near tip stress and strain fields. The path independent nature of the integral allows an integration path, Γ, sufficiently far from the crack tip, to be substituted for a path close to the crack tip region. Rice proved path-independence of the J-integral for a material model obeying deformation theory of plasticity. Hayes (1970) showed that for incremental plasticity theory the J-integral demonstrates approximate path-independence within the plastic region.

Experimental determination and evaluation of the J-integral were conducted by Begley & Landes (1972) and Landes & Begley (1972). They presented how the J-integral can be experimentally determined from the load-deflection diagram. They proposed that the J-integral could be used as a ductile fracture criterion, subject to certain not-well-defined limitations. They provided experimental evidence suggesting that fracture initiation could be correlated with attainment of a critical J value in a wide but limited range of specimen sizes and geometries. Different specimen configurations develop different crack tip fields. For example, surface-edge-cracked bend specimen (SE(B)) exhibits a high triaxial tension on the plane ahead of the crack, while center-cracked panel (CCP) develops straight 45° slip-lines proceeding from the crack tips to the free surfaces. Different crack tip fields affect the microstructural mechanisms of ductile cracking, void growth and coalescence. The nonuniqueness in crack tip fields determined from small strain formulations was found for the nonhardening idealisation. When strain hardening was included, asymptotic analysis led to crack tip singular fields which were unique to within a scalar amplitude factor and the J-integral served as a measure of this amplitude (McMeeking & Parks, 1979). Begley & Landes (1972) argued that since virtually all materials exhibit some strain hardening, J should characterize the near-tip fields at least up to the beginning of crack extension.

The foundation of the J-integral is on the static component of the ‘energy-momentum tensor’, introduced by Eshelby (1956) to characterize generalized forces on dislocations and point defects in elastic fields (Rice, 1968). In a two-dimensional elastic body the value of the J-integral is often connected to the value of the partial derivative of the potential energy (Π) with respect to the crack length, a (Rice, 1968), Eq. 5.

$$J = -\frac{\partial \Pi}{\partial a} \tag{5}$$

However, Santaoja (1992 and 1996) has shown that the crack tip singular field in elastic medium contributes an additional term to Eq. 5. Santaoja criticized the validity of Eq. 5 for cases where small-scale yielding conditions exist at the crack tip. He also reminded that the potential energy (Π) is a concept of pure elastic deformation and conservative loading. Thus, independent of the scale, no material dissipation, e.g. plastic yielding, is allowed to exist when potential energy is examined (Santaoja, 1996).

McMeeking & Parks (1979) proposed specimen size limitations for J testing requiring all specimen dimensions to exceed $M \cdot J/\sigma_0$, where M = 25...50 for bend and CT-specimens and M = 200 for center-cracked panels. They argued that the imposition of size or deformation limitations for J is more or less arbitrary due to gradual loss of J-dominance as load increases. An alternative technique leading to similar conclusions was developed by Shih & German (1981) who compared the asymptotic plastic field of cracks in tension and bending with the HRR field.

Specimen size limitations are related to the loss of constraint at the crack tip stress fields due to specimen boundary effects. In the following, approaches for constraint description currently in use are presented.

3 METHODS FOR CONSTRAINT CORRECTION

3.1 T-STRESS

Larsson & Carlsson (1973) analysed finite element models of various cracked specimens and compared the results with the results obtained from a boundary layer model. They studied the point of the loading where the first element in the model starts to yield in a linearly elastic - ideally plastic material and found out that the stress intensity factor at the beginning of the yielding is specimen geometry dependent. Thus, the boundary layer model was not capable to describe accurately crack tip deformation in real specimens made of low strain hardening material and the first term in the expansion (Eq. 1) was not sufficient to describe the crack tip fields in different cracked geometries. Larsson & Carlsson (1973) concluded to present the stress field very much like in Eqs. 1 and 2, but they denoted the non-singular components as T and divided it to a constant and a r-dependent component, Eq. 6.

$$\sigma_{ij} = \frac{K_I}{(2\pi r)^{1/2}} f_{ij}(\theta) + T_{ij0} + T_{ij\infty}(r) \tag{6}$$

In Eq. 6 only the T_x component (to the direction of the crack, on the crack plane) of T_{ij0} is non-zero. The T_x for various geometries can be determined as a difference in x-direction stress determined by using the specimen geometry model and boundary layer model (blm), Eq. 7.

$$T_x = \sigma_x(r,0)_{specimen} - \sigma_x(r,0)_{blm} \tag{7}$$

Rice (1974) studied further the effect of T-stress on fracture parameters. He discovered that the T-stress has no effect on the J-integral, but positive (negative) T-stress decreases (increases) plastic zone size and CTOD compared to the previous models not including the T-stress effect. Rice (1974) also suggested use of a new non-singular stress parameter, S, for the three-dimensional analyses. S would act perpendicular to the principal plane of deformation influencing the transition to a non-plane strain yielding mode involving through-thickness deformation. In general, $S = \nu T$.

Harlin & Willis (1988) investigated few cracked geometries analytically and applied both theoretical cleavage and ductile failure criteria to find out the transition from the brittle to ductile fracture as a function of temperature, assuming that temperature has effect principally on flow stress. They found a scale effect dependent on fracture criterion. If fracture toughness was assumed to depend on critical normal stress, the crack could have been ten times smaller than if the fracture was assumed to depend on critical hydrostatic stress, to be still determined by the stress intensity factor, K. In other words, the introduction of non-singular T- and S-stress affected the size limit of a ‘long’ crack, characterized solely by K.

For a boundary layer model of radius R, Harlin & Willis (1988) presented a relation between T-stress and the stress intensity factor, Eq. 8.

$$T_1 = t'\left(\frac{R}{a}\right)^{\frac{1}{2}} \frac{K_I}{(\pi R)^{\frac{1}{2}}}, \tag{8}$$

where t' is the biaxiality coefficient. The relation between T_1-term and the singular stresses to be applied at the boundary r = R of the boundary layer mesh demonstrates the relative importance of T_1 as the crack size decreases. For cracks which are sufficiently small, the boundary layer formulation ceases to provide a representation for the near-tip field in a specimen, because attainment of a specified K_I would require an applied stress large enough to cause plasticity to spread far from the crack tip. However, there is an intermediate range of crack sizes for which the T_1-effect is both significant and representative of specimen behaviour.

Harlin & Willis (1988) supposed that practical applications may involve competition between a negative T_1-stress and a positive S_3-stress. An example was provided by a semicircular surface flaw, loaded by a thermal shock induced by rapid surface cooling. This would induce biaxial tension in planes parallel to the surface and hence the value of S_3 at the deepest point of the flaw would contain a contribution from the tensile stress normal to the plane of the flaw. The T_1-stress would likely be negative as in the case of the edge crack in plane strain. Which non-singular term would dominate is unknown.

Leevers & Radon (1983) introduced a biaxiality parameter B, through which the T-stress is defined, Eq. 9.

$$B = \frac{T\sqrt{\pi a}}{K} \tag{9}$$

Bilby et al. (1986) investigated the effect of the second-order term on large geometry change deformation field within 2·CTOD. Negative T-stresses were shown to reduce the level of maximum hydrostatic stress ahead of the crack. Void growth rate decreased and ductility enhanced due to the loss of triaxiality ahead of the crack tip.

Betegòn & Hancock (1991) correlated loss of J-dominance with the second term in the asymptotic expansion of the elastic field. They characterized the effect of the T-stress on the small-strain region surrounding the blunting zone. In this context, the loss of J-dominance was associated with compressive (negative) T-stresses which introduce a corresponding second-order term into the nonlinear asymptotic expansion, of which the HRR field is simply the first term. The second-order term causes the stresses ahead of the crack to fall for negative T-stresses while remaining close to the HRR field for positive T-stresses and maintaining J-dominance. Single parameter characterization (J-dominance) was

thus concluded to be a feature of geometries which show positive biaxiality parameters (B). Specimens which have negative biaxialities were predicted to loose J-dominance at a deformation level which depends on T. The biaxiality parameter, B, is a specimen configuration dependent parameter. Values of B for various specimen geometries are presented by Leevers & Radon (1983) and Al-Ani & Hancock (1991).

Betegòn & Hancock (1991) approximated the effect of T-stress on hoop stress as:

$$\frac{\sigma_{\theta\theta}}{\sigma_0} = \left(\frac{\sigma_{\theta\theta}}{\sigma_0}\right)_{T=0} + a_1\left(\frac{T}{\sigma_0}\right) + a_2\left(\frac{T}{\sigma_0}\right)^2 \text{, for } T/\sigma_0 < 0, \qquad (10)$$

where the a_i:s depend on strain hardening exponent, n.

Al-Ani & Hancock (1991) analysed edge-cracked bars in tension and bending. The ratio of the crack depth to the specimen width, a/W, seemed to govern the J-dominance. In bend specimens with a/W < 0.3 and in tension-loaded specimens with a/W < 0.5, the J-dominance was lost, associated with the development of plasticity to the cracked face before full ligament plasticity. Specimens with deeper cracks seemed to maintain the J-dominance until large-scale plasticity, because plasticity developed through the ligament without spreading to the cracked face. Again, the loss of J-dominance was attributed to compressive T-stresses, while specimens which exhibited tensile T-stresses retained J-dominance in accord with modified boundary layer formulations. It should be noted that for the shallow cracks the J-dominance was lost before $a < 200 \cdot J/\sigma_0$, which is earlier than proposed by McMeeking & Parks (1979) for deeper cracks.

Du & Hancock (1991) represented numerical results of modified boundary layer formulations as slip-line fields. The full Prandtl field was achieved with tensile T-stresses which caused plasticity to appear on the crack flanks and envelope the crack tip. The stresses were independent of T as further deformation could not change the flow field or the stress level at the crack tip. The crack tip stress $\sigma_{\theta\theta}$ directly ahead of the crack was 0.5% and 0.1% lower than the Prandtl value ($2.97 \cdot \sigma_0$) for T=0 and T=0.443, respectively, the deviation being dependent on material parameters such as Poisson's ratio, ν. This situation corresponds to the non-hardening limit of the HRR field characterized by J. Compressive T values were shown to reduce the stress triaxiality within the plastic zone at the crack tip. This effect was associated with the appearance of an elastic wedge at the crack flanks, so that plasticity did not completely envelope the crack tip and the stress field required two-parameter characterization.

Sham (1991) presented how T-stress can be determined by the so-called second order weight functions through a work-conjugate integral. He presented tabulated T-stress values for various specimen configurations.

Tvergaard & Hutchinson (1994) applied an elastic-plastic crack growth model, with a traction-separation law specified on the crack plane to characterize the fracture process, to study the effect of T-stress on fracture resistance. They discovered that with compressive T-stresses the plasticity contributes significantly to crack growth resistance even at low peak stress values. As compressive T-stress increases from zero to the yield strength the plasticity effect increases radically and crack growth resistance increases. The increase of tensile T-stress from zero to half of the yield strength produces only a negligible decrease in crack growth resistance. These results are in accord with results of Du & Hancock (1991). Operational range of T-stress was discovered to be from zero to negative T-stresses, while changes in T-stress in the tensile range have only small effects on fracture toughness.

Hancock et al. (1993) tested a series of cracked specimen configurations to correlate the geometry dependence of crack tip constraint in full plasticity. They found that at a small crack extension the toughness is dependent on the crack tip constraint determined by T. The loss of constraint in center-cracked panels increases radically as crack grows, compared to constraint loss in 3PB specimens, due to the effect of constraint on the slope of the resistance curves. By use of the T-stress the resistance to crack tip tearing of very dissimilar configurations can be placed in order. An enhanced geometry dependent toughness and resistance to tearing was found to associate with specimens of negative T-stress.

Parks (1991) discussed the three T-terms which arise in 3-D crack problems. He generalized the T-stress effect on linear elastic stress distribution in the vicinity of the crack front location:

$$\lim_{r\to 0}\begin{bmatrix}\sigma_{11} & \sigma_{12} & \sigma_{13}\\ \sigma_{21} & \sigma_{22} & \sigma_{23}\\ \sigma_{31} & \sigma_{32} & \sigma_{33}\end{bmatrix}=\frac{K_I}{\sqrt{2\pi r}}\begin{bmatrix}f_{11}(\theta) & f_{12}(\theta) & f_{13}(\theta)\\ f_{21}(\theta) & f_{22}(\theta) & f_{23}(\theta)\\ f_{31}(\theta) & f_{32}(\theta) & f_{33}(\theta)\end{bmatrix}+\begin{bmatrix}T_{11} & 0 & T_{13}\\ 0 & 0 & 0\\ T_{31} & 0 & T_{33}\end{bmatrix} \quad (11)$$

He also proposed an equivalent stress, T^e, corresponding to T_{ij}. In the form of Eq. 12, the T^e does not violate the von Mises yield criterion based on yield stress, σ_0:

$$\sigma_0 > \sqrt{\left(T_{33}^{\ 2} - T_{11}T_{33} + T_{11}^{\ 2} + 3T_{13}^{\ 2}\right)} \equiv T^e \quad (12)$$

3.2 Q-PARAMETER

O'Dowd & Shih (1991 and 1992) developed the idea of a J-Q annulus. Within the J-Q annulus the full range of high- and low-triaxiality crack tip stress and strain fields are shown to be members of a family of crack tip field solutions parameterized by Q when distances are measured in terms of J/σ_0. The stress distribution and the maximum stress depend on Q alone while J sets the size scale

over which large stresses and strains develop. The Q-family provides a framework for quantifying the evolution of constraint as plastic flow progresses from small-scale yielding to fully yielded conditions.

O'Dowd & Shih (1991) analysed a boundary layer model in which the remote tractions were given by the two term linear-elastic solution, Eq. 13.

$$\sigma_{ij} = \frac{K_I}{\sqrt{2\pi r}} f_{ij}(\theta) + T\delta_{1i}\delta_{1j} \tag{13}$$

For a fully yielded crack geometry, they presented the stress, strain and displacement fields in the form:

$$\sigma_{ij} = \sigma_0 f_{ij}\left(\frac{r}{J/\sigma_0}, \theta; Q\right), \quad \varepsilon_{ij} = \varepsilon_0 g_{ij}\left(\frac{r}{J/\sigma_0}, \theta; Q\right), \quad u_i = \frac{J}{\sigma_0} h_i\left(\frac{r}{J/\sigma_0}, \theta; Q\right) \tag{14}$$

where f_{ij}, g_{ij} and h_i depend on dimensionless combinations of material parameters.

For a linear-elastic, power-law hardening material they presented the following two-term expansion for mode I stresses within the small-strain formulation for distances sufficiently close to the crack tip but still outside the zone of finite strains:

$$\frac{1}{\sigma_0}\begin{pmatrix}\sigma_{rr} & \sigma_{r\theta}\\ \sigma_{r\theta} & \sigma_{\theta\theta}\end{pmatrix} = \left(\frac{J}{\alpha\varepsilon_0\sigma_0 I_n r}\right)^{1/(n+1)}\begin{pmatrix}\tilde{\sigma}_{rr} & \tilde{\sigma}_{r\theta}\\ \tilde{\sigma}_{r\theta} & \tilde{\sigma}_{\theta\theta}\end{pmatrix} + Q\left(\frac{r}{J/\sigma_0}\right)^q\begin{pmatrix}\hat{\sigma}_{rr} & \hat{\sigma}_{r\theta}\\ \hat{\sigma}_{r\theta} & \hat{\sigma}_{\theta\theta}\end{pmatrix} \tag{15}$$

The second-order term in Eq. 15 was obtained by subtracting the applied J scaled HRR distribution from the two-term expansion (Eq. 13), which was assumed to be the exact solution. The examination of the second-order term revealed that $0 < q < 0.071$ for $4 \le n \le 20$. Thus, the r-dependence of the second-order term could be neglected and Eq. 15 approximated:

$$\frac{1}{\sigma_0}\begin{pmatrix}\sigma_{rr} & \sigma_{r\theta}\\ \sigma_{r\theta} & \sigma_{\theta\theta}\end{pmatrix} = \left(\frac{J}{\alpha\varepsilon_0\sigma_0 I_n r}\right)^{1/(n+1)}\begin{pmatrix}\tilde{\sigma}_{rr} & \tilde{\sigma}_{r\theta}\\ \tilde{\sigma}_{r\theta} & \tilde{\sigma}_{\theta\theta}\end{pmatrix} + Q\begin{pmatrix}\hat{\sigma}_{rr} & \hat{\sigma}_{r\theta}\\ \hat{\sigma}_{r\theta} & \hat{\sigma}_{\theta\theta}\end{pmatrix}, \tag{16}$$

where Q is essentially a stress triaxiality parameter, since second-order stress terms on the diagonal are almost equal and off-diagonal terms are relatively small on the angular sector $|\theta| < \pi/2$. A negative Q value decreases hydrostatic stress by $Q\cdot\sigma_0$ from the Q = 0 reference state and a positive Q value has an inversed effect. This can be written as:

$$\sigma_{ij} = (\sigma_{ij})_{HRR} + Q\sigma_0\delta_{ij}, \text{ for } r > J/\sigma_0 \text{ and } |\theta| < \pi/2 \tag{17}$$

The second, hydrostatic term in Eq. 17 is independent of distance and angle. Xia et al. (1993) showed that the second term actually represents the effect of the four

higher order terms in the elastic-plastic near-tip fields, while O'Dowd (1995) stated that the number of higher order terms needed depends on applied constitutive relation. The Q values for many different geometries have been presented by O'Dowd & Shih (1994).

To extend the validity of Eq. 17 it was expressed by means of the SSY solution which matches the HRR stress distribution at $r/(J/\sigma_0) = 2$ and $\theta = 0$ as the $Q = 0$ distribution, Eq. 18 (O'Dowd & Shih, 1991). The Q value is always determined at $r/(J/\sigma_0) = 2$, which is outside the finite-strain region, but still within the J-Q annulus. The J-Q annulus is defined as the region of outer boundary $r_{J\text{-}Q}$, where Eqs. 17 and 18 accurately describe the field.

$$\sigma_{ij} = (\sigma_{ij})_{Q=0} + Q\sigma_0\delta_{ij}, \text{ for } r > J/\sigma_0 \text{ and } |\theta| < \pi/2 \qquad (18)$$

The SSY reference distribution $Q = 0$ in Eq. 18 is not applicable for accurate quantification of the field near and within the finite-strain region for studies of micromechanisms of fracture. For such applications the reference distribution should be obtained from a finite-deformation analysis. However, for distances $r/(J/\sigma_0) > 2$ the difference between the finite- and small-strain $Q = 0$ distributions is negligible. Also, the difficulty with material description is avoided by taking the SSY solution as a reference solution (O'Dowd, 1995). Equation 18 has been found to be a good description of the fields even for materials which do not display power-law hardening. If a high constraint measure, J_{Ic}, is to be used as the reference toughness, then use of SSY field ($T = 0$) as the reference distribution is sensible, because this is the field which specimen experiences rather than the HRR field (O'Dowd, 1995). To better take into account the constitutive relation, O'Dowd (1995) added a third, strain hardening dependent, term to Eq. 17:

$$\sigma_{ij} = (\sigma_{ij})_{HRR} + a_0(n)\cdot\sigma_0\delta_{ij} + Q\sigma_0\delta_{ij}, \text{ for } r > J/\sigma_0 \text{ and } |\theta| < \pi/2 \qquad (19)$$

Operationally, Q can be defined as the difference between the full-field solution for $\sigma_{\theta\theta}$ and the HRR field at $r/(J/\sigma_0) = 2$ and $\theta = 0$:

$$Q \equiv \frac{\sigma_{\theta\theta} - (\sigma_{\theta\theta})_{HRR}}{\sigma_0}, \text{ at } \theta = 0 \text{ and } r = 2J/\sigma_0 \qquad (20)$$

Q can be evaluated from any of the stress components and at any angle in the forward sector $\pi/2 < \theta < 3\pi/2$, but for definition the $\sigma_{\theta\theta}$ is a sensible choice.

O'Dowd & Shih (1991) studied biaxially loaded center-cracked panels and 3PB specimens and found out that the Q value depends on the geometry and extent of plastic yielding. For certain crack geometries Q reaches a steady-state value when fully plastic conditions are approached. $-2 < Q < 0.2$ covered every stress distribution that was generated. They suggested that not only the fracture toughness but also the resistance curve could be determined as a function of Q

[$J_c(Q)$ and $J_R(\Delta a,Q)$]. Different specimen configurations could be placed on a single toughness curve as a function of the Q-parameter.

From dimensional analysis (O'Dowd & Shih, 1992) deduced a one-to-one correspondence between T-stress and Q-parameter:

$$Q = F(T/\sigma_0; n), \tag{21}$$

where F additionally depends weakly on dimensionless combinations of material parameters. Equation 21 is valid only when remote stresses are applied by Eq. 13. They define a K-T annulus as a region bounded by $r_{K\text{-}T}$, where fields are accurately descibed by Eq. 13. They also define that under SSY conditions the plastic zone lies well within the K-T annulus. The relation between Q and T-stress is approximated by Eq. 22, which applies primarily for n = 5...10, but the dependence of the Q-parameter on strain hardening exponent is weak.

$$Q = a_0 + a_1\left(\frac{T}{\sigma_0}\right) + a_2\left(\frac{T}{\sigma_0}\right)^2, \tag{22}$$

where a_i:s are dependent on n. The resemblance of Eqs. 10 and 22 should be noted. O'Dowd & Shih (1994) extended the expression in Eq. 22 to a cubic form, deleted the constant term and defined a_i:s to be functions of strain hardening exponent, n:

$$Q = a_1(n)(T/\sigma_0) + a_2(n)(T/\sigma)^2 + a_3(n)(T/\sigma_0)^3 \tag{23}$$

They also presented the parameters a_i tabulated.

Ainsworth & O'Dowd (1994) proposed simple relationships for T and Q, which are not dependent on strain hardening, Eq. 24. These relationships are actually equivalent to what has been suggested by Du & Hancock (1991) for elastic-perfectly plastic materials:

$$Q = T/\sigma_0 \text{ when } T/\sigma_0 < 0 \quad \text{and} \quad Q = 0.5T/\sigma_0 \text{ when } T/\sigma_0 > 0 \tag{24}$$

O'Dowd & Shih (1992) presented that for finite-width crack geometries under large-scale yielding conditions Eq. 21 is not applicable, because Q depends also on remote loading and specimen geometry:

$$Q = G\left(\frac{J}{L\sigma_0}; n, geometry\right), \tag{25}$$

where L is the relevant crack dimension.

O'Dowd & Shih (1992) analysed center-cracked panels (CCP) with varying biaxiality ratios and 3PB specimen configurations with various crack lengths. For CCP:s the stress and strain fields strongly resembled members of the Q-family.

The resemblance persisted for distances up to approximately $r/(J/\sigma_0) = 5$. However, the excessive crack-tip blunting resulted in a reduced zone of J-Q dominance. Despite the reduction, the J-Q annulus was considerably larger than the J-annulus.

For 3PB geometry with a/W = 0.1 the Q behaviour was very much like in CCP:s, but for 3PB geometry with a/W = 0.5 there seemed to be a reduction in J-Q annulus at fully yielded conditions ($J/\sigma_0 > 0.05b$). This was explained to be due to global bending stress distribution decreasing the zone of dominance of the crack tip stress field. For a/W = 0.5 and 0.7, Q was sensitive to the choice of distance at extensive yielding and under these circumstances the Q value is not well defined (O'Dowd & Shih, 1992).

O'Dowd & Shih (1992) introduced J_c^{∞}, which refers to the value of J_c for a long crack ($a \rightarrow \infty$). J_c^{∞} corresponds to the value of J_c under SSY conditions when T = 0. Somewhat related to the SSY correction method (see section 3.3) they express the ratio of the two J values:

$$\frac{J_c}{J_c^{\infty}} = \left(\frac{\frac{\sigma_c}{\sigma_0} - Q}{\frac{\sigma_c}{\sigma_0} - Q_{T=0}} \right)^{n+1} \tag{26}$$

In Eq. 26 the decrease of Q value associated with the loss of constraint increases the apparent J value depending exponentially on the strain hardening exponent. Interestingly, the constraint loss is not dependent on the distance from the crack tip, r.

O'Dowd (1995) generated J-Q toughness curves for initiation of cleavage fracture and ductile tearing. A simple cleavage toughness locus may be constructed based on the attainment of a critical hoop stress at a critical distance ahead of the crack. Assuming that the critical distance r_c is within the J-Q annulus, a fracture toughness curve is obtained:

$$J_c = J_{Ic}\left(1 - \frac{Q}{\sigma_c/\sigma_0 - a_0}\right)^{n+1}, \tag{27}$$

where a_0 is from Eq. 19 and J_{Ic} is the toughness measured in a specimen with Q = 0. For initiation of ductile tearing O'Dowd (1995) postulated a critical crack tip opening criterion:

$$\delta_c = d(n,Q)\frac{J_c}{\sigma_0}, \tag{28}$$

where $0.5 < d < 1$, for n = 10. By taking $\delta_c = 0.5 \cdot J^d_{Ic}/\sigma_0$, where J^d_{Ic} is the J value at which ductile tearing initiates when Q = 0 and re-arranging the terms, led to:

$$\frac{J_c}{J^d_{Ic}} = \frac{1}{2 \cdot d(n,Q)} \tag{29}$$

3.3 SMALL-SCALE YIELDING CORRECTION (SSYC)

Dodds et al. (1991) and Anderson & Dodds (1991) investigated the specimen size requirements in the brittle-to-ductile transition region. They utilized elastic-plastic finite element analysis to quantify the size dependence of cleavage fracture toughness and developed size criteria for single-parameter fracture toughness characterization. Crack tip stress fields obtained from specimens of finite size were compared to the corresponding stress fields obtained from a small-scale yielding model. Critical J and CTOD values, relative to the small-scale yielding value, were predicted as a function of specimen size, strain hardening exponent and ratio of crack depth to specimen width, a/W. They studied 3PB specimen configurations with a/W ranging from 0.05 to 0.5 and strain hardening exponent of a Ramberg-Osgood power law expression ranging from 5 to 50.

Dodds et al. (1991) took into account the micromechanism of cleavage fracture. Most of the micromechanical models (for example Wallin et al., 1984a and b) are based on the statistical weakest-link theory, which assumes that cleavage failure is controlled by the largest or most favourably oriented fracture-triggering particle, involving a local Griffith instability of a microcrack. The instability criterion implies fracture at a critical normal stress near the tip of the crack. The size of the volume under critical normal stress affects the probability of cleavage fracture through the nature of statistical existence of a critical microstructural feature near the crack tip.

Finite deformation analyses for the SSY model and for 3PB specimens with a/W = 0.5 by McMeeking & Parks (1979) predicted the location of maximum tensile stress on the crack plane at approximately 2...4·CTOD ahead of the deformed crack tip. Thus, the fracture process zone for cleavage fracture lies beyond the neighbourhood of the blunted crack tip and the region over which the asymptotic HRR field is adequate to describe the stress distribution (Dodds et al., 1991). Differences in stresses for the SSY model predicted by the notch tip blunting analyses and by the small-strain analyses become negligible for r > 2...3·CTOD. These observations supported use of the small-strain theory for predicting the stress fields ahead of the crack tip for stress-controlled cleavage fracture process. For cleavage fracture Anderson & Dodds (1991) suggested that stress fields at 2...10·CTOD should be taken into consideration when comparing the SSY model and finite configurations. Thus, the finite-element mesh refinement must be adequate for this purpose.

In two-dimensional plane-strain analysis the area under critical normal stress around the crack tip can be expressed as a function of the applied J-integral:

$$A(\sigma_1/\sigma_0) = \phi \frac{J^2}{\sigma_0^{\ 2}} h(\sigma_1/\sigma_0), \tag{30}$$

where ϕ is a constraint factor, dependent on the applied stress and specimen geometry and the function h is integrated around the crack tip. $\phi = 1$ for the SSY solution and $\phi < 1$ for finite specimen configurations. The effective J-integral, J_{SSY}, in large-scale yielding relates the area inside the principal stress contour to the small-scale yielding case:

$$A(\sigma_1/\sigma_0) = \frac{J_{SSY}^{\ 2}}{\sigma_0^{\ 2}} h(\sigma_1/\sigma_0) \tag{31}$$

The J_{SSY} in Eq. 31 is the value of a finite geometry J that would result in the area A, if the crack tip plastic zone was small compared to other dimensions. From Eqs. 30 and 31 the ratio between the two J values can be expressed as:

$$\frac{J_{finite}}{J_{SSY}} = \sqrt{\frac{1}{\phi}} \tag{32}$$

When generated for specific material properties and specimen sizes, results of the form in Fig. 1 can be used to scale fracture toughness data between specimen configurations. The curves serve two purposes: the geometry dependence of fracture toughness data for various different a/W ratios through correlations to a single a/W ratio or to the SSY model and commonly available test results for standardized, deeply notched specimens may be scaled for assesment of shallow flaws (Dodds et al., 1991). However, use of Fig. 1 for scaling purposes for real defects is still theoretical due to commonly complex 3-dimensional shapes of real flaws.

The evolution of fracture toughness for various specimen configurations in Fig. 1 permits a relatively straight-forward construction of the relationship between stresses in finite specimens and SSY model for a given material and geometry:

$$\sigma_i^{\ FINITE} = \sigma_i^{\ SSY} \cdot H_i\left(\frac{J_{FINITE}}{J_{SSY}}\right), \tag{33}$$

where the functions H_i, defined using stress on the symmetry plane, for example, are represented by curves in Fig. 1 (Dodds et al., 1991).

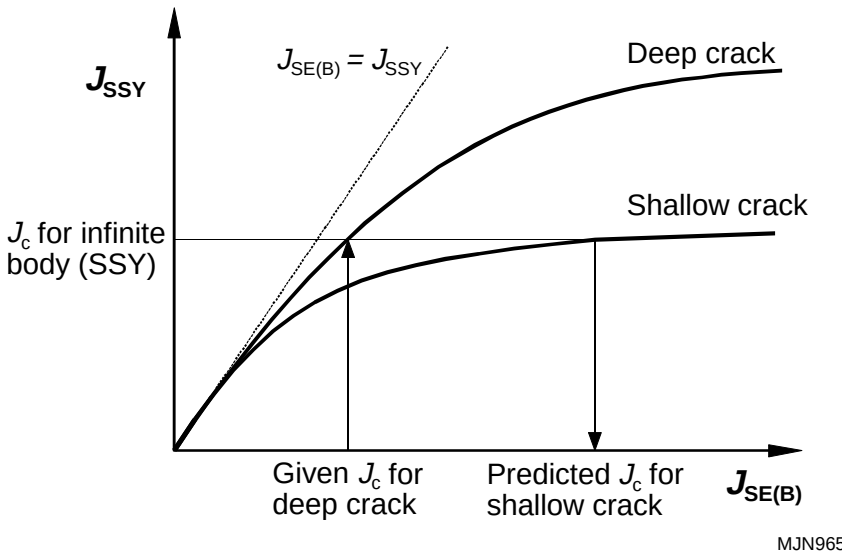

Figure 1. Scaling models for SE(B) specimens with different a/W ratios (Dodds et al., 1991).

Dodds et al. (1991) plotted the shapes of the constant principal stress contours at various loading levels for both SSY and 3PB models. The shape of the contours in non-dimensionalized coordinates proved to be identical within the limits of finite element mesh refinement for all analysed models and loadings, while the contour size (in non-dimensionalized coordinates) in finite configurations decreased as loading was increased. This implies that the SSY stress fields can be written as a product of two separable functions of crack tip coordinates r and θ:

$$\sigma_{ij} = c\left(\frac{J}{\sigma_0 r}\right) d_{ij}(\theta) \tag{34}$$

This relationship appeared to be valid for 2·CTOD < r < 20·CTOD.

The J/J_{SSY} ratio at a fixed J value seemed to be insensitive to the principal stress value used for determining the contour. Thus, it seemes that critical applied J values could be corrected for constraint loss by means of a single scaling factor: the applied J and J/J_{SSY} ratio seemed to completely characterize the principal stress distribution ahead of the crack tip. Also, the scaling factor seemed to be insensitive to the r and θ coordinates.

For every specimen configuration and strain hardening combination there seemed to be a saturation point after which the effective driving force for cleavage fracture did not increase as loading was increased. After the saturation point, the likelihood for cleavage fracture decreased potentially and was possible only after some ductile tearing bringing more material to be sampled for finding a fracture triggerer, as previously shown by Wallin (1985).

Anderson & Dodds (1991) recommended following specimen size limits for cleavage fracture in deeply notched bend specimens:

$$B, b, a \geq \frac{200 \cdot J_c}{\sigma_Y} \tag{35}$$

or

$$B, b, a \geq 300 \cdot \delta_c \tag{36}$$

These size requirements are significantly less stringent than those of standard ASTM E399-90 for K_{Ic} determination, but more restrictive than size requirements of standard ASTM E813-89 for J_{Ic} determination.

4 METHOD FOR THICKNESS CORRECTION

The cleavage fracture model involves cracking of some brittle particle in a grain or its boundary and subsequent crack growth into the adjacent grains. Thus, the cleavage fracture of a cracked specimen requires two conditions: existence of a brittle particle within the crack tip process zone and high enough stress state to break the particle and drive the crack into surrounding grains. The distribution of the brittle particles in a material sample is random. Increasing the material volume statistically increases the number of the brittle particles in that volume. The size of the volume within the crack tip process zone, where existence of the brittle particles is critical with respect to the cleavage fracture, depends on the size of the principal stress contour ahead of the crack tip where stress is higher than cleavage fracture stress and on the specimen thickness which determines the length of that contour in the specimen thickness direction, i.e. the volume.

Ritchie et al. (1973) investigated the relation between local fracture criterion and macroscopic fracture toughness for 4-point-bend specimens with sharp precracks, at a wide temperature range. The significant feature was that cleavage stress level was exceeded locally at the crack tip even before fracturing, so that not only the value of σ_f but also the size scale over which the fracture criterion was met was considered. They also studied how size of the finite radius of the notch tip affects the microstructurally significant length scale compared to the fatigue precrack.

Batdorf & Crose (1974) developed a weakest-link theory for macroscopically homogeneous isotropic material containing randomly oriented microcracks uniformly distributed in a location, assuming that fracture depends only on macroscopic stress normal to the crack plane. They expanded as a Taylor series a function representing the number of cracks per unit volume failing at a specific value of normal stress. They obtained the coefficients for the Taylor series from tensile tests, but their ultimate goal was to incorporate the obtained model into a FEM code to be able to analyse computationally also multiaxial stress states.

Evans (1978) developed a general approach for the statistical analysis of fracture under multiaxial stress state, but in a mathematically less complicated way than Batdorf & Crose (1974). Evans (1978) invoked a critical coplanar strain-energy release-rate fracture criterion and considered distributions of penny-shaped cracks in random and preferred orientations.

Beremin (1983) introduced the Weibull stress σ_w (Weibull, 1939) as a fracture parameter. Beremin (1983) derived a local criterion for the prediction of cleavage fracture based on analyses of a wide range of experiments and finite element calculations for a nuclear pressure vessel steel. Under SSY conditions, the cumulative failure probability criterion was found to predict correctly the temperature dependence of K_{Ic} as well as the size effect on fracture toughness. Also, Beremin (1983) applied the model for multiaxial stress states as

implemented in a computer program. He obtained good results in predicting the warm prestress effect in completely yielded specimens.

Mudry (1987) extended the approach of Beremin (1983) with plane-strain finite element analyses to include large-scale yielding effects on the Weibull stress. Size and deformation limits for fracture testing followed from deviation of the specimen Weibull stress from small-scale yielding values.

Wallin et al. (1984a) presented the WST-model, in which they assumed that statistically distributed carbides control fracture toughness. They presumed that macroscopic fracture nucleates in a volume between the crack tip and elastic-plastic boundary. They used the Griffith crack advancement criterion as a fracture criterion and considered the radius of the carbide as a critical factor with respect to the probability of cleavage fracture initiation.

The probability for cleavage fracture initiation in case of a sharp crack according to Wallin et al. (1984b) can be written as:

$$P_f = 1 - e^{-\left(\frac{K_I - K_{\min}}{K_{0B} - K_{\min}}\right)^4}, \tag{37}$$

where P_f is the fracture probability, K_I is the stress intensity, K_{min} is a lower limiting fracture toughness (≈ 20 MPa√m for steels) and K_{0B} is a thickness and temperature-dependent normalization factor. For a constant temperature condition Wallin et al. (1984b) wrote:

$$K_{B_1} = K_{\min} + \left(K_{B_2} - K_{\min}\right)\left(\frac{B_2}{B_1}\right)^{\frac{1}{4}}, \tag{38}$$

where B_1 and B_2 are respective specimen thicknesses.

Wallin (1984) applied Eq. 38 to fracture toughness test results of a brittle ceramic (SiC) material. He discovered very promising results; with 88 data points, the 90% accuracy of the analysis was as good as 4%. Additionally, Wallin (1985) applied Eq. 38 to results of various metallic materials in the literature and discovered further proof for the validity of the formula.

Recasting Eq. 38 in terms of J yields:

$$J_{c-(2)} \approx J_{c-(1)}\left(\frac{B_{(1)}}{B_{(2)}}\right)^{\frac{1}{2}}, \tag{39}$$

where the J equivalent of K_{min} has been neglected as a small term ($J_{min} << J_{c-(1)}$). The development of the model assumes that each point along the crack front experiences the same local J value and corresponding SSY stress field.

5 APPLICATION OF METHODS

In this chapter conducted tests, computational analyses and application of constraint correction methods to the test and analysis results are summarized. Detailed test and analysis methodologies are described in the appended papers, while here the scope and scale of the conducted research to some extent is presented.

5.1 EXPERIMENTAL AND COMPUTATIONAL ANALYSES

The research consisted of a wide scale of test and analysis applications. The experimental programme included both static and dynamic testing, while the characteristic specimen dimension ranged from 5 mm to 300 mm. The flaw types in the specimens were typically straight, through thickness cracks, but also a set of specimens with elliptical surface cracks was included. Computational analyses consisted of 3-dimensional linear and non-linear finite-element analysis of 3PB-, CT- and surface flawed specimens, while the 3PB- and CT-specimens were also analysed 2-dimensionally. The research programme is summarized in Tables 1 - 3. In Table 3 is summarized the characteristic dimension ratios of investigated through-thickness cracked specimens.

Table 1. The experimental programme.

Dynamic tests:	Impact tests at the brittle-to-ductile transition and upper shelf regions with fatigue precracked and side-grooved 10·10·55 mm 3PB specimens with approximate a/W = 0.05, 0.1, 0.3 and 0.5. The test material was A533B Cl. 1 pressure vessel steel.
Static tests:	4PB testing of fatigue precracked specimens with a/W = 0.5, while the width and length of the specimens were 40 mm and 200 mm, respectively. The specimen thicknesses were 5, 10, 20, 100, 200 and 300 mm and the three thinnest configurations were totally 20% side-grooved. The test temperature was at the brittle-to-ductile transition region and the test material was moderate hardening structural steel.
	4PB testing of plates with elliptical surface cracks. The relative specimen dimensions were aimed to be the same as for the second 4PB plate in Table 2. The brittle-to-ductile transition curve was determined and the test material was mild steel. A transition curve for the material was also obtained by testing standardized 25 mm thick 3PB specimens.

Table 2. The computational analysis programme. (lin. = linear analysis, non-lin. = non-linear analysis, n = strain hardening exponent. For 3PB- and CT-specimens: W = width, B = thickness, a = crack length, S-G = side-grooved (n = 10). For 4PB plates: c = half of the crack width, b = half of the specimen width, t = specimen thickness.)

3PB Specimens

	a/W = 0.1	a/W = 0.5
W/B = 1	lin., non-lin. (n = 5, 10, 20)	lin., non-lin. (n = 5, 10, 20)
W/B = 2	lin., non-lin. (n = 5, 10, 20), S-G	lin., non-lin. (n = 5, 10, 20), S-G
W/B = 4	lin., non-lin. (n = 5, 10, 20)	lin., non-lin. (n = 5, 10, 20)
Plane-strain	lin., non-lin. (n = 5, 10, 20)	lin., non-lin. (n = 5, 10, 20)

CT-Specimens

	a/W = 0.6
W/B = 1	lin., non-lin. (n = 5, 10, 20)
W/B = 2	lin., non-lin. (n = 5, 10, 20), S-G
W/B = 4	lin., non-lin. (n = 5, 10, 20)
Plane-strain	lin., non-lin. (n = 5, 10, 20)

4PB plates with elliptical cracks

	b/t = 2
a/c = 0.357, c/b = 0.175, a/t = 0.125	lin., non-lin. (n = 10)
a/c = 0.333, c/b = 0.375, a/t = 0.25	lin., non-lin. (n = 10)

Table 3. The matrix of characteristic dimension ratios of investigated through-thickness cracked specimens (DYN = dynamic testing, STAT = static testing and FEA = finite element analysis).

	B/W= 0.125	**0.25**	**0.5**	**1.0**	**2.5**	**5.0**	**7.5**
a/W=0.05				DYN			
0.1		FEA	FEA	FEA DYN			
0.3				DYN			
0.5	STAT	FEA STAT	FEA STAT	FEA DYN	STAT	STAT	STAT
0.6		FEA	FEA	FEA			

5.2 APPLIED CONSTRAINT CORRECTIONS

5.2.1 Impact tests

The T-stress for each test result was calculated by the formula given by Kirk et al. (1993), Eq. 40.

$$T = 1.5 \cdot \frac{PS}{BW^2} \cdot \beta(a/W) \cdot \left[\frac{1.99 - \frac{a}{W}\left(1 - \frac{a}{W}\right)\left(2.15 - 3.93\frac{a}{W} + 2.7\left(\frac{a}{W}\right)^2\right)}{\sqrt{\pi}\left(1 + 2\frac{a}{W}\right)\left(1 - \frac{a}{W}\right)^{1.5}} \right], \quad (40)$$

where

$$\beta(a/W) = -0.462 + 0.461\left(\frac{a}{W}\right) + 2.47\left(\frac{a}{W}\right)^2 \quad \text{for } 0.025 \le a/W \le 0.9 \quad (41)$$

Kirk et al. (1993) obtained Eq. 41 by fitting a polynom to the data of Al-Ani & Hancock (1991), who reported β as a biaxiality parameter. By combining Eqs. 9 and 41 and K solution for an SE(B) specimen with a span-to-width ratio of 4:1 by Tada et al. (1985), Kirk et al. (1993) obtained Eq. 40 for the linear relation between T-stress and applied load, P.

The Q parameter was determined based on the Q - $J/(a\sigma_0)$ relations for SE(B) specimens with strain hardening exponent n = 10 by O'Dowd and Shih (1992).

The SSY correction of the test results was obtained according to Anderson & Dodds (1991). J_{SSY} was calculated according to function in Eq. 42, in which parameters A and m were provided by Dodds (1991).

$$\frac{J}{J_{SSY}} = 1 + \left(A \cdot \frac{J}{a\sigma_Y} \right)^m \quad (42)$$

Additionally, data was analysed by taking into consideration the fracture probability based on the statistical cleavage fracture model by Wallin (1991).

5.2.2 Static tests

Thickness effect

In the original, not thickness-corrected data the thickness effect is evident as apparent fracture toughness increases with decreasing thickness. The side-grooving did not seem to affect constraint in thickness direction in a detectable amount.

Two methods were applied in attempts to remove the thickness effect: the method based on statistical probability of cleavage fracture (Wallin, 1991) and the method based on effective thickness derived from 3-dimensional FE-analysis by Dodds (1993).

Elliptical flaws

For the plate specimens with elliptical flaws no method to determine the specimen fracture toughness nor geometrical constraint correction was available. The FE-analysis results of the plate specimens were utilized in deriving an equation for the fracture toughness and for taking into account the constraint and thickness effect. For comparison, standardized 25 mm thick 3PB specimens of the same material were also tested in order to compare the results.

5.2.3 Computational analyses

SSY-correction and J-Q approach were applied to results of both 2- and 3-dimensional non-linear FE-analyses summarized in Table 2. The stress, strain and displacement output of each node from the FE-program were given as input to complicated FORTRAN post-processing programs which calculated and plotted required constraint parameters. The calculation was basically done 2-dimensionally, while for 3-dimensional models the calculation was conducted for each planar layer separately. The planar layers were in normal planes with respect to the crack front in each front position both in through thickness and elliptical crack models. The FORTRAN-code consisted basically of routines for calculating the presentative stresses and strains and their related parameters and the relations presented by O'Dowd & Shih (1991, 1992) and Anderson & Dodds (1991).

6 RESULTS

6.1 PLASTIC η-VALUES

The η_{pl} values for Eq. 43 were determined from non-linear FE-analyses as η_{max} and η_{avg} corresponding to maximum η_{pl} value at the crack front and crack front average value, respectively. η_{pl} was determined based both on plastic load-line displacement (lld-pl) and plastic CMOD (δ-pl) (Appendix 1).

$$J = J_{el} + J_{pl} = \frac{K_I^{\,2}(1-\nu^2)}{E} + \eta_{pl}\frac{U_{pl}}{bB}\ , \qquad (43)$$

where J_{el} and J_{pl} denote the elastic and plastic contributions to J and U_{pl} defines the unrecoverable plastic work of the applied load.

In deep notch SE(B) and CT specimens, η_{pl} values for thickness average J agreed well with those found in plane-strain analyses and with those in current testing standards. Only a small effect of strain hardening was detected. The 3-dimensional η_{pl} values based on lld-pl for shallow notch SE(B):s revealed approximately 20 - 25% variation over the hardening range (n = 5...20), while η_{pl} values based on δ-pl showed only a 4 - 5% variation (Appendix 1).

The η_{max} value corresponding to maximum J value for all SE(B) and CT specimens was calculated at the center of the crack front, except for one configuration: a/W = 0.1 and W/B = 1, for which η_{max} (and correspondingly highest constraint) occurred approximately at $x_3/(B/2) = 0.53$ location (Appendix 1).

The plastic η values were also derived for the surface cracked plates. The η_{pl} seemed to behave in an inverse way compared to the SE(B) and CT specimens, because η_{pl} decreased with increasing crack depth.

6.2 T-STRESS

Based on the results of dynamic fracture toughness tests, T-stress is a linear-elastic parameter best suited for constraint indexing. Low a/W specimens with large compressive T-stress produced high apparent fracture toughnesses, while deep notched configurations with zero or somewhat tensile T-stresses gave low, more material dependent toughness results. Perhaps unexpected was that apparent fracture toughness began to distinctly increase at quite high compressive T-stress values, T/σ_0 level being approximately -0.7. At lower T/σ_0 ratios, the T-stress lost its influence, since plastic deformation and in some cases even ductile tearing began to considerably increase measured fracture toughness values far beyond values measured with specimens behaving more in a linear-elastic way. However,

T-stress provided a good base for estimating the level of scatter in apparent J_c values as a function of initial specimen dimensions for sufficiently high a/W ratios, although it was not able to give quantitative estimates (Appendices 3 and 4).

6.3 J-Q TRAJECTORIES

3-dimensional FE-analyses revealed that for the deep notch SE(B) and CT specimens, Q values are positive at low loads except near the outside surface (Figure 2). Over the center portion of the specimen thickness, $Q \geq 0$ condition existed strictly for deformation levels $b > 140 \cdot J_{avg}/\sigma_0$ (for W/B = 1 and n = 10), while larger deformation produced negative Q values. The plane-strain results for this configuration indicated constraint loss at lower levels of deformation, $b > 170 \cdot J/\sigma_0$. Q values at various distances ahead of the crack tip on the midplane showed steadily increasing radial dependence under increasing load. All deep notch SE(B) and CT specimens exhibited similar levels of Q dependence on r at large deformations (Appendix 1).

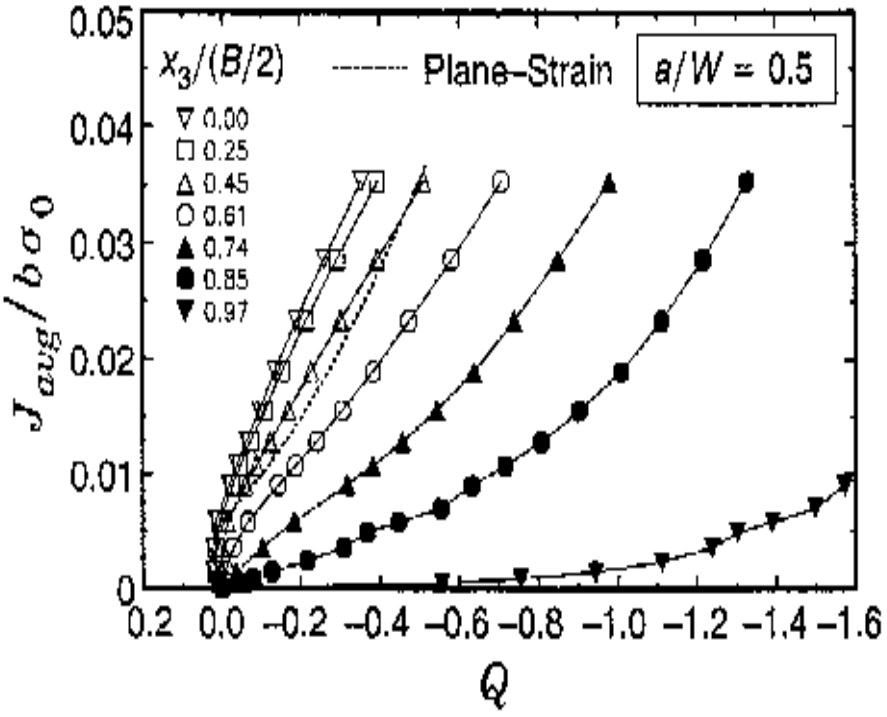

Figure 2. Constraint in terms of Q-parameter for plane-sided, deep notch (a/W = 0.5) SE(B) specimen having W/B = 1 and n = 10 (Publication 1).

Q values for the a/W = 0.1 SE(B) configurations revealed an immediate loss of constraint upon loading (Figure 3). The plane-strain results agreed reasonably well with the W/B = 1 configuration. The Q values were much more radial-distance independent than for deep notch configuration. No practical size or deformation limit existed to maintain Q ≥ 0 condition after load was applied, while all of the shallow notch J-Q trajectories fell within a relatively narrow band of very low constraint (Appendix 1).

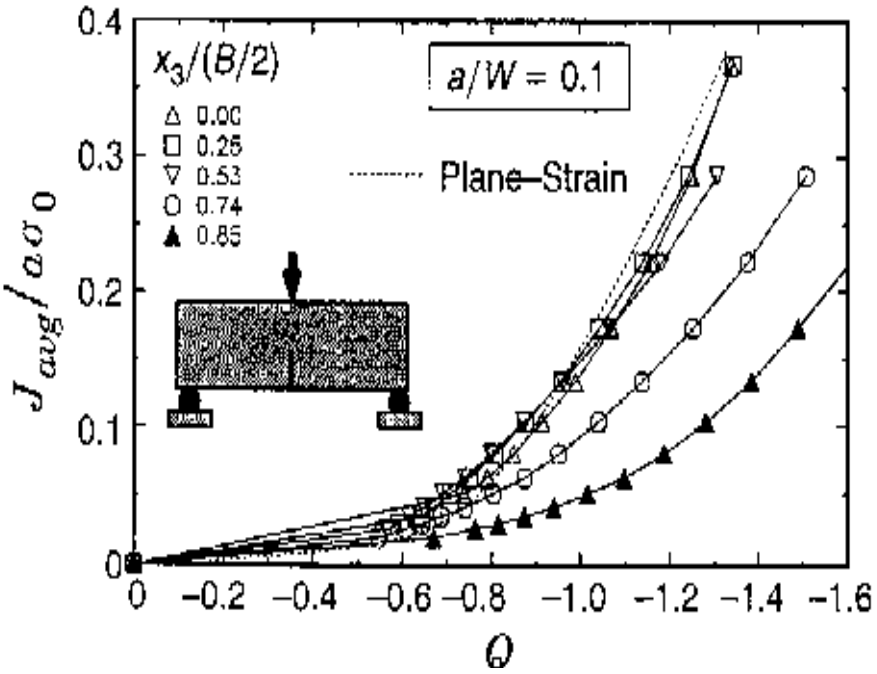

Figure 3. Constraint in terms of Q-parameter for plane-sided, shallow notch (a/W = 0.1) SE(B) specimen having W/B = 1 and n = 10 (Publication 1).

Following observations were made for SE(B) specimens in Appendix 1: (1) the deep notch W/B = 1 and 2 trajectories are nearly identical for n =10 with a somewhat larger difference for n = 5; (2) side grooves in the W/B = 2 deep and shallow notch configurations provide small increases of constraint on the midplane at high deformation levels and have insignificant effect early in the loading; (3) deep notch specimens having W/B = 4 show a severe constraint loss on the midplane upon initial loading while the relative effect in shallow notch configurations is much less severe; (4) all of the shallow notch J-Q trajectories fall within a relatively narrow band of very low constraint; (5) strain hardening variations from n = 5 to 10 have a small effect on the 2-dimensional and 3-dimensional trajectories at higher loads - for a specified J value, reduced hardening makes Q more negative. Further examination revealed that strain hardening influences the J-Q trajectories most strongly at low-to-moderate loads.

The results of J-Q trajectories for CT specimens led to following observations: (1) side grooves have a slight effect of lowering constraint at high load levels on the specimen midplane; (2) side grooves increase constraint significantly at other locations relative to the plane-sided specimen; (3) strain hardening affects constraint somewhat for the standard W/B = 2 specimen at high loads with a larger effect for the thinner specimen (W/B = 4); (4) $Q \geq 0$ conditions exist strictly for deformation levels $b > 100 \cdot J_{avg}/\sigma_0$ in the standard W/B = 2 configuration. The increased elastic T-stress of the CT specimen relative to the deep notch SE(B) specimen leads to the 25% increase in deformation before SSY conditions break down (Appendix 1).

The J-Q trajectories showed that Q values close to the side surface of the deep notched SE(B) specimen fall below values obtained close to free surface of the surface cracked specimens in bending, which is probably due to constraining of the uncracked surface next to the crack. At the center of the crack front, the Q values for elliptical surface cracks are negative straight upon loading, while Q is more negative for the shallower crack. As loading increased, the Q-values for surface cracks began to saturate to a constant level. For both examined surface cracks, there seemed to be a relatively narrow scatter for J-Q trajectories corresponding to the center portion of the crack front, while behaviour of the J-Q trajectories closer to the free surface clearly deviated from that behaviour. The shape of the J-Q trajectories for the shallower surface crack early in the loading showed similar behaviour as those for the shallow notch SE(B) specimen. It seems obvious, that J-Q trajectories are well suited for the analysis of the constraint evolution in the elliptical surface cracks under bending loading (Appendix 2).

Experimentally, the Q-parameter for small Charpy-size impact specimens was not very effective in describing constraint. J-Q relationship was different for each configuration, although scatter especially between a/W = 0.5 and a/W = 0.3 configurations was not large. However, the initial Q value predicted poorly the obtained fracture toughness for an individual specimen based on a/W. Results indicated that for this type of specimens under dynamic loading, the fracture toughness is not solely a function of the Q-parameter (and geometry), but also a function of the J-level. This observation decreases the quantitative nature of the Q-parameter and presents it more as a qualitative indexing parameter, in the same way as T-stress for these specimens (Appendices 3 and 4).

6.4 TOUGHNESS SCALING MODEL (= SSYC)

6.4.1 Analysis results

All deep notch SE(B) specimens showed a strong dependence on $\bar{\sigma}_c$ once large-scale yielding conditions began to prevail, but with a smaller dependence with higher strain hardening (Figure 4). Strain hardening had a much greater relative effect on the toughness scaling model than on the J-Q trajectories once SSY broke down. For SE(B) specimens with lower strain hardening, large increments of applied J were needed to produce small changes in J_0 values. The dependence of the scaling model on $\bar{\sigma}_c$ at very large deformations makes attempts to correct for constraint loss in deep notch SE(B) specimens questionable, although it appeared that for moderate-to-high hardening materials useful engineering approximations are possible at deformation levels in the range $J_{avg}/b\sigma_0 \approx 0.01$ - 0.015. The scaling model clearly maintained sufficient independence of $\bar{\sigma}_c$ early in the loading to support proposals for size/deformation limits ($b > M \cdot J_{avg}/\sigma_0$) to insure SSY conditions at fracture although the gradual loss of constraint introduces subjectivity into the process (Appendix 1).

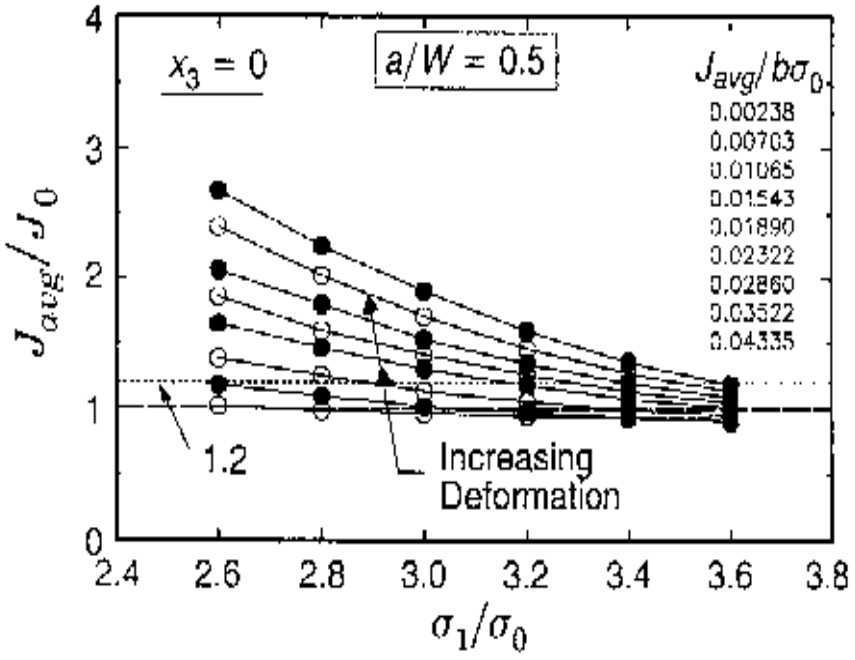

Figure 4. Dependence of toughness scaling ratio on specified principal stress value for plane-sided, deep notch (a/W = 0.5) SE(B) specimen having W/B = 1 and n = 10 (Publication 1).

For all the shallow notch SE(B) configurations, applications of the scaling model to correct for constraint loss appeared much more promising with a strong independence on $\bar{\sigma}_c$ to J_{avg}/J_0 ratios approaching 6-7 and 4-5 for n = 10 and 5, respectively (Figure 5). The 3-dimensional scaling models were in relatively good agreement with the plane-strain results (Appendix 1).

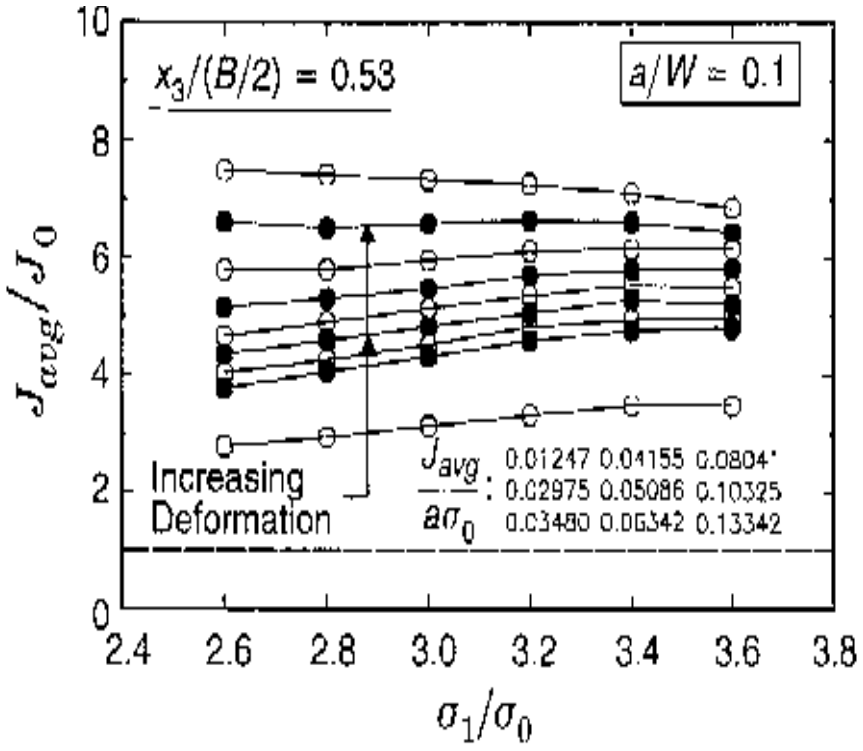

Figure 5. Dependence of toughness scaling ratio on specified principal stress value for plane-sided, shallow notch (a/W = 0.1) SE(B) specimen having W/B = 1 and n= 10 (Publication 1).

The CT specimens responded essentially in the same way as deep notch SE(B) specimens with very minor effects of the side grooves on the scaling model on the midplane. The plane-strain results matched better the 3-dimensional results than in the case of deep notch SE(B) specimens (Appendix 1).

The scaling models for the two studied elliptical surface cracks showed deviation from the SSY behaviour well before deep notch SE(B) specimen, while the larger surface crack maintained SSY conditions up to larger crack front averaged deformation, J_{avg} (Figure 6). The scaling models seemed to describe constraint of the surface cracks reasonably well. The transition from the better SSY conditions following behaviour at the center of the crack to almost no-constraint conditions close to the surface was quite smooth for the large surface crack, while for the shallower crack the behaviour at the center of the crack front departed clearly from the behaviour closer to the free surface. The scaling models in terms of the average J at the whole crack front seemed to be dependent on the maximum crack depth (Appendix 2).

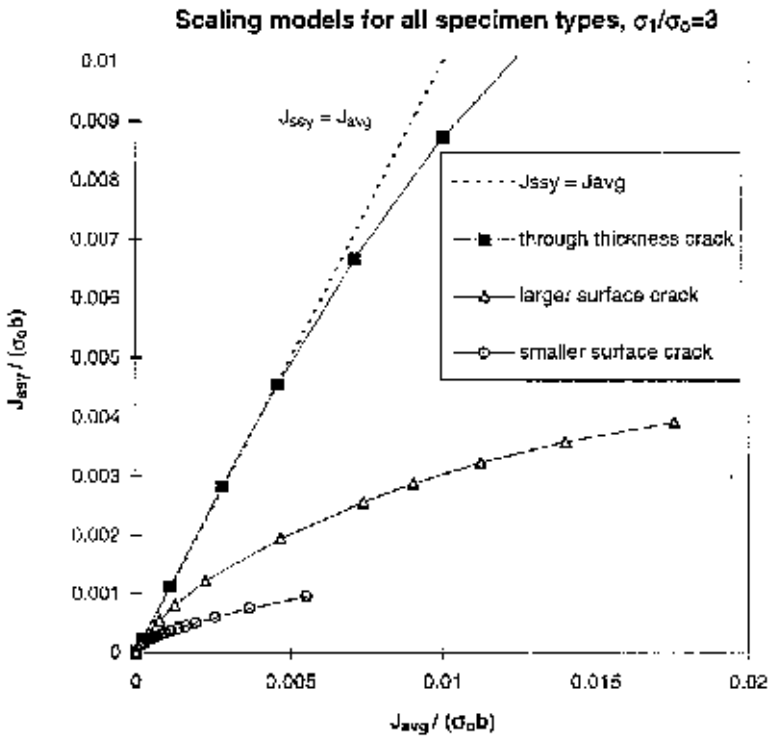

Figure 6. The toughness scaling models for the surface cracks in a plate and the through thickness crack in SE(B) specimen. The ratio of the principal stress to the yield stress is 3.0. b is the ligament length of the SE(B) specimen (= 25.4 mm) (Publication 2).

The toughness scaling models based on plane-strain static analyses corrected surprisingly well the constraint variation in experimental impact tests with fatigue precracked Charpy-size specimens with varying a/W ratio. This observation gave further confidence for the SSY correction method as a real experimentally applicable method for constraint correction, since it succeeded in the task where T-stress and Q-parameter did not manage as well. Together with the statistical treatment, the SSYC method presented the obtained data in a homogeneous form with little scatter (Appendices 3 and 4).

6.4.2 Specimen size requirements

The maintenance of SSY conditions over a substantial part of the specimen thickness to higher J levels than found in the plain-strain analyses indicated that M = 200 limit (Eq. 35) on measured J_c values for deep notch specimens may be

lowered to M ≈ 50-75 for moderate hardening, which brings the analytically determined value into closer accordance with the experimental observations (Appendix 1).

When considering the specimen size limit based on 3-dimensional toughness scaling models, the M-factors corresponding to strict SSY, 10% and 20% deviation from the SSY conditions (Eq. 44) were determined for deep notch SE(B) and CT specimens (Appendix 1).

$$b \geq M_{(1.0,1.1,1.2)} \cdot \frac{J_{avg}}{\sigma_0} \tag{44}$$

When compared to M = 200 in Eq. 35, even the strict SSY M-values ($M_{1.0}$) for high-to-moderate hardening materials (n = 5 and 10) are clearly less stringent. Of all M-values determined for investigated 3-dimensional configurations, only $M_{1.0}$ for low hardening material (n = 20) SE(B) specimen is more stringent than M = 200. All other M-values approve much smaller specimen dimension for fracture toughness determination.

In all cases, the CT specimens had smaller M values than corresponding SE(B) specimens having the same W/B and n, which imply the maintenance of SSY conditions to greater levels of deformation (Appendix 1).

6.5 THICKNESS EFFECT

The 3-D analyses revealed much greater through-thickness variations in crack front stresses for deep notch specimens than for shallow notch specimens. Stress triaxiality on the specimen midplane of deep notch specimens remained at SSY levels to higher local J values than indicated by the plane-strain models. Crack front stresses near the outside surfaces of plane-sided specimens fell well below midplane levels and plane-strain levels (Appendix 1).

For shallow-notch SE(B)s with W/B = 1 and 2, the plane-strain analyses provided remarkably good descriptions of stresses ahead of the crack tip; this lack of thickness effect perhaps explains the surprisingly good J-Q correlations and toughness constraint corrections for such specimens.

The statistical treatment for the experimental results of static tests with strongly varying specimen thickness proved to be very good. The treatment was able to present test results well within the confidence limits of 5% and 95% fracture probability (Appendix 4).

6.5.1 Effective thickness

A 3-dimensional form of the toughness scaling model is proposed which reflects both the statistical effects of volume sampling due to thickness differences and the

constraint loss on crack-front stress fields due to large scale yielding. At a given loading level determined by J, a specific principal stress contour $\sigma_1/\sigma_0 = \bar{\sigma}_c$, encloses the tip at each location at the crack front. A(s, $\bar{\sigma}_c$) denotes the area σ_c enclosed by the contour, which lies in the principal normal plane to the crack front location s along the front. At location s = s_{max}, the enclosed area attains a maximum value $A_{max} \equiv A(s_{max}, \bar{\sigma}_c)$. The volume of material along the crack front over which the principal stress exceeds $\bar{\sigma}_c$ is given for a straight crack front by Eq. 45 (Appendix 1).

$$V(\bar{\sigma}_c) = \int_{-B/2}^{B/2} A(s, \bar{\sigma}_c) ds \qquad (45)$$

The replacement of the actual specimen thicknesses appearing in Eq. 39 with effective thicknesses, $B_{eff} = V/A_{max}$ is suggested. In most studied configurations A_{max} occurred at the center of the specimen, but not in every case. The front location at which A_{max} occurs has the maximum 'in-plane' constraint and the B_{eff}/B defines the equivalent fraction of the specimen thickness subjected to that constraint level. It was shown that B_{eff}/B decreased from near unity under linear elastic conditions, for plane-sided specimens, to nearly deformation independent value once large-scale yielding conditions prevailed. Moreover, B_{eff}/B remained reasonably insensitive to a range of realistic $\bar{\sigma}_c$ values. The B_{eff}/B ratio varied significantly with W/B for fixed a/W and n: the ratio decreased with increasing W/B, while greater amount of strain hardening elevated values of B_{eff}/B. For low a/W SE(B) specimen, the side grooving increased B_{eff} relatively more than for deep notched SE(B) and CT specimens due to initially low overall in-plane constraint in low a/W configurations.

For non-side grooved SE(B) specimens, values of B_{eff}/B lied in the range of 0.4 - 0.8 with a dependence on the a/W and W/B ratios and material flow properties. Perhaps surprisingly for specimens with side grooves, B_{eff}/B exceeded slightly the value of the corresponding plane-sided specimen even though the front length decreased by 20%.

The concept of B_{eff} can be extended to correlate surface crack and through thickness crack configurations. This has been conducted in Appendix 2, where the ratio of the effective and real crack front lengths proved to be higher for the surface cracked plates than for the 3PB specimen.

6.5.2 Development of thickness correction

To accommodate the potentially strong influence of constraint loss from 'in-plane' effects, a replacement of $J_{c-(1)}$ in Eq. 39 with $J_0(J_{c-(1)})$ is proposed, where J_0 is calculated by plane-strain SSY analyses. A measured fracture toughness, J_c, is then constraint and thickness corrected to a SSY condition with a convenient reference thickness ($B = B_{ref}$) by using the formula:

$$\bar{J}_0 = J_0(J_c) \cdot \sqrt{B_{eff} / B_{ref}} \ , \qquad (46)$$

where the quantity B_{ref} may be assigned a convenient value of 25 mm, which is in accord with specifications of current standards for fracture toughness determination. The corrected set of $\overline{J}_0$ values from different specimens are then given equal weight in further statistical treatments of toughness values to define confidence bounds etc. (Appendix 1).

The key features of the development include the reasonably strong independence of B_{eff}/B and $J_0(J_c)$ on the selected $\overline{\sigma}_c$ for low constraint specimen configurations in most need of the correction. In deep notch SE(B) and CT specimens, SSY conditions often exist on the midplane at fracture and only the effective thickness correction is required. For these specimens, B_{eff}/B remains reasonably independent on σ_c. Finally, given a value of $\overline{J}_0$ for the material, the corresponding J_c-value for a specific fracture specimen may be computed by using the reverse of the above described process: the B_{eff}/B and $J_0(J_c)$ corrections must be known for the fracture specimen (Appendix 1). In Appendix 2 an attempt has been made to correlate surface cracked plate results with 3PB specimen results by using Eq. 46.

6.6 FRACTURE TOUGHNESS FOR SURFACE CRACK

Based on the 3-dimensional FE analyses for the two studied surface cracks, a formula for the calculation of surface crack fracture toughness was proposed in Appendix 2 (Eq. 47). The elastic part was based on work of Newman & Raju (1984), while the plastic part was based on work done by momentum through plastic straining, normalized by the ligament area. The empirical results provided verification to the formula.

$$J_{tot} = \frac{K_{e,avg}^{\ 2}}{E'} + \eta \cdot \frac{Mom \cdot \varepsilon_{pl}}{t \cdot 2b - \frac{\pi}{2} \cdot a \cdot c} \qquad (47)$$

7 DISCUSSION

7.1 SIGNIFICANCE OF RESULTS

This thesis work falls into the very active research area of present fracture mechanics. It includes the comparison of the three most common methods for constraint description with and without statistical thickness correction. The usefulness of the methods has been first verified and then the two most powerful methods for constraint characterization, the J-Q locus and the SSY correction, have been studied in detail by applying 3-dimensional finite element analyses. The conducted 3-dimensional analyses are direct development to the 2-dimensional analyses, on which the characterization of crack-tip stress distribution has been previously based on. Based on the analyses, significant results of the in-plane constraint conditions were obtained and new M-factors were introduced (see Eq. 46), which are one basis in the development of the new ASTM standard proposal for fracture toughness determination in the transition range. The same analysis methodologies have been applied also to the semielliptical surface crack extending the current knowledge of surface crack characterization and correlation with through-thickness crack geometries. In short, the work presented in this thesis is focused on currently significant problems of fracture mechanics and can be seen as one step towards understanding the transferability of fracture mechanical quantities.

7.2 ASSESSMENT OF RESULTS

Narasimhan et al. (1988) have undertaken numerical finite element and experimental interferometric investigation to assess 3-dimensional effects and HRR dominance near a crack front in a ductile 3-point bend specimen. The excellent agreement between numerical and experimental results assured them of the correctness of their calculations. Despite differences in the material parameters ($n = 22$ and $\sigma_0 = 1030$ MPa) the through thickness variation of the J-integral and CTOD correlate well with the results of Publication 1 (Appendix 1). Similar results have been also reported by Nakamura et al. (1989) and Brocks & Olschewski (1986). DeLorenzi & Shih (1983) and Faleskog (1994) found an abrupt increase in J value close to the side-grooved surface of a CT-specimen. Same observation was made also in Publication 1. It seems that a side-groove acts as a stress concentrator when deformation is primarily elastic, but with increased loading the J at the specimen center begins to grow faster and becomes more critical than the J close to the side-groove. It seems that all 3-dimensional finite element results of standardized specimens support each other, but the refinement of the analyses of Publication 1 makes them special and unique. The finite element analysis is always a discretization of the real structure, which brings some error to the results. The error decreases with the refinement of the model, but never vanishes completely. Also, modelling of the nonlinear behaviour is not exact.

The modelled SE(B) specimens have been 50.8 mm wide, while thickness has ranged from 12.7 mm to 50.8 mm. The results seem to scale very well, since the SSYC of Publication 1 corrects the results of two different size specimens equally well in Figs. 7 and 8. In Fig 7 are presented the original and the SSY-corrected results of Publications 3 and 4 (W = B = 10 mm) and in Fig. 8 are some original and SSY-corrected results of the HSST program (W = 100 mm and B = 50...100 mm). The material has been A533B Cl. 1 steel in both studies. The material properties in the development and production phases in Fig. 8 are different due to the heat treatment, so the thickness effect can not be evaluated.

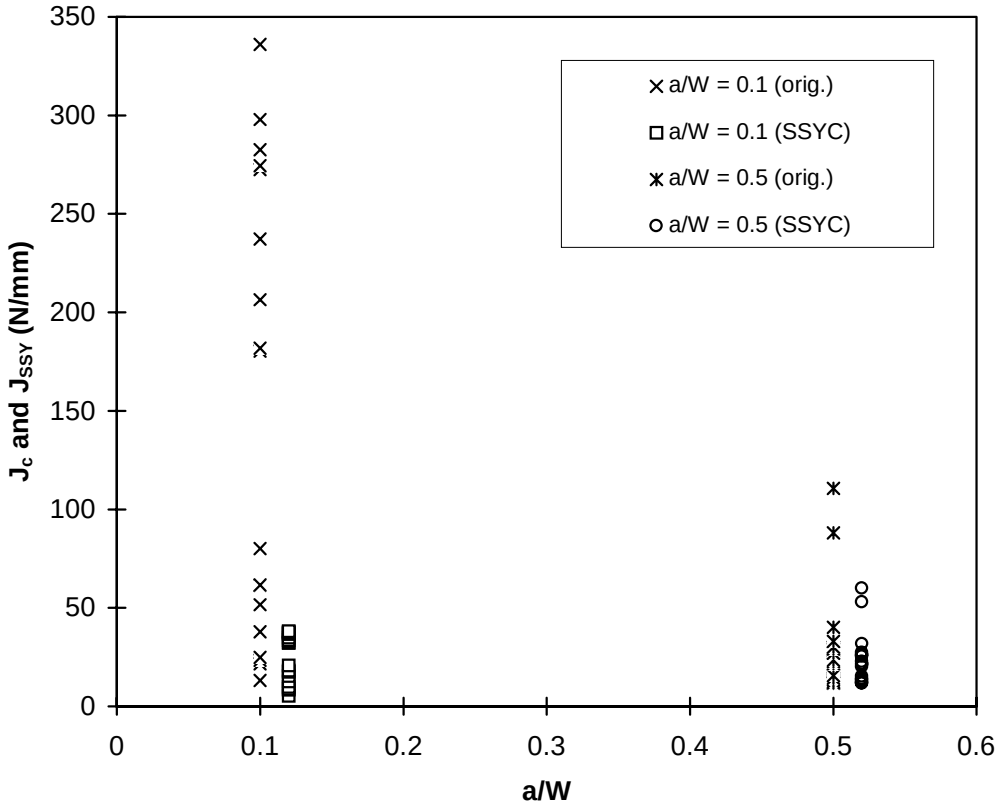

Figure 7. Original and small-scale yielding corrected impact test results. The original results are from Publications 3 and 4 (Appendices 3 and 4), while the SSYC is based on 3-d results given in Publication 1. The SSYC data points have been shifted at a/W axis for clarity.

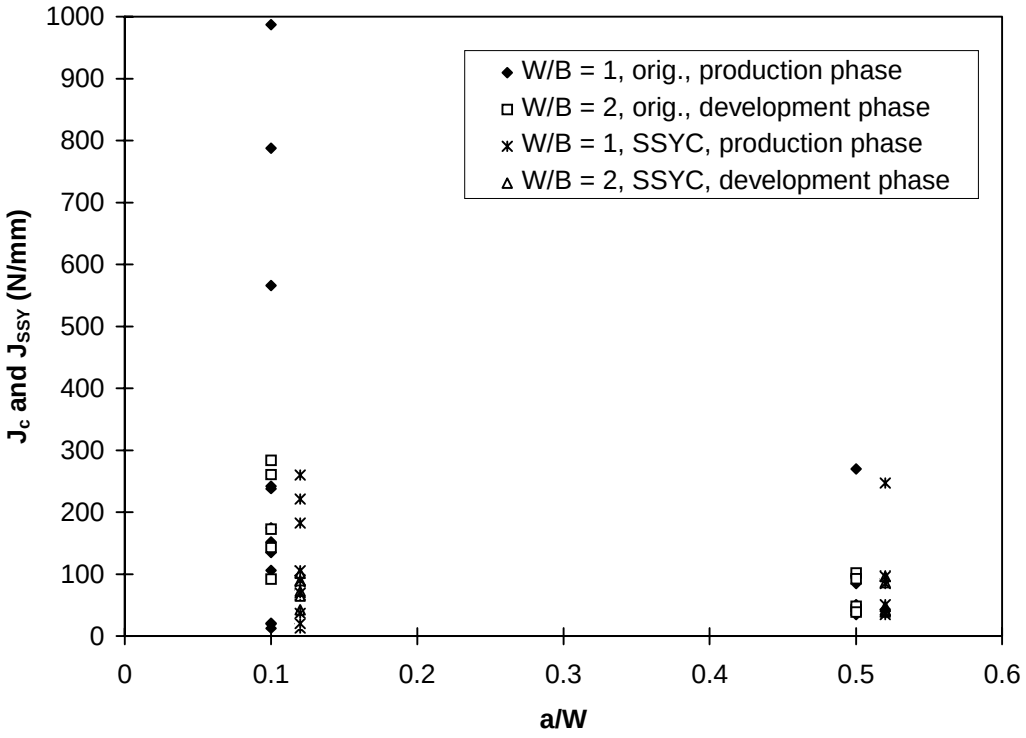

Figure 8. The original and small-scale yielding corrected test results of the HSST program. The original results are presented by Theiss et al. (1994) and the SSYC is based on results of Publication 1. The SSYC data points are shifted at a/W axis for clarity.

There are not many published 3-dimensional elastic-plastic analyses of surface cracks, and most of them deal with surface crack in a plate or pipe under tension or combined tension-bending loading. The author could not find any other 3-dimensional nonlinear finite element analysis of a surface cracked plate under four-point-bending, so the assessment of the results is conducted by comparison to results obtained from slightly different analyses.

Parks & Wang (1988) and Parks (1990) analysed both semicircular and semielliptical surface cracks in a plate under remote tension loading. They discovered that the J distributions along the crack front in these crack types are clearly different, but for a specific crack type the change in strain hardening exponent (n = 5 to 10) or in remote stress level does not affect J distribution significantly. They showed that low remote stress level for a semielliptical surface crack creates relatively higher J value at and close to the free surface ($\phi < 15°$) than high remote stress level, which agrees with the observation in Publication 2 (Appendix 2). Same kind of result is also presented by Franco & Gilles (1992), who analysed 3-d surface cracks under pure bending in elastic-plastically behaving pipe. Franco & Gilles found out that the J-integral at the deepest point of the crack front is always higher than J at the surface and that the ratio increases with increasing applied loading. Kumar & German (1988) present limited results of the same kind, obtained both with 3-d FEM and elastic-plastic estimation method for

a semielliptical crack in the inside surface of a pipe under remote tension loading. Faleskog et al. (1991) obtained also a same kind of J distribution for a combined tension-bending loaded plate with a semielliptical surface crack. Overall, investigated 3-d elastic-plastic analyses of a surface crack under tension or bending loading give very similar results supporting and verifying each other.

The FE-analysis of a surface crack does not differ much from the analysis of a standardized through-thickness crack specimen. The biggest difference is the modelling of the crack front, while rest of the analyses can proceed in a similar way. One way to assure oneself that there are no significant errors in the model is to run a linear-elastic analysis and compare results with the results of Newman & Raju (1984). Newman & Raju give stress-intensity factor solutions for a variety of curved crack shapes under several loading types and are widely referenced in the literature. In the finite element models of Publications 1 and 2 only the model geometry has been changed, while rest of the analysis procedures are identical. Thus, the differences in the crack-tip behaviour are only due to the geometry. Same arguments about the discretization and refinement errors apply for the surface crack analysis as for the through-thickness crack analysis.

8 CONCLUSIONS

Detailed 3-dimensional finite element analyses have been conducted for standardized surface-edge cracked 3-point bend specimen (SE(B)), compact-tension specimen (CT) and surface-cracked plate in 4-point bending. The effect of specimen and flaw size and material hardening properties have been extensively analysed to reveal their effect on specimen constraint behaviour, characterized by toughness scaling models and J-Q trajectories.

Experimental tests for a wide range of specimen and flaw types have been conducted to verify effectiveness of constraint correction and indexing methods currently in use. Also, a statistical treatment has been applied for specimen thickness effect.

Based on FEM analyses on standardized specimens, specimen size limitations for brittle-to-ductile transition region have been proposed. Use of an effective thickness (B_{eff}) for average constraint correction has been suggested and a development for the statistical treatment procedure has been proposed and applied for investigated specimen geometries.

Conducted experiments proved that small-scale yielding correction (SSYC) and statistical treatment for specimen thickness effect are applicable for specimen size correction in actual specimens, while T-stress and Q- parameter seemed to serve better as qualitative indexing parameters.

Based on FEM analysis for elliptical surface cracks in plates under bending and verified by conducted experiments, a formula for fracture toughness calculation for the plate was proposed.

Comparison of in-plane behaviour in analysed specimens proved that J-Q approach and SSYC are well applicable for FEM-based analysis of constraint behaviour. Surface crack was found to loose its constraint well before deep notch SE(B) specimen in terms of applied deformation, while size of the surface crack seemed to govern its constraint behaviour.

Based on the results, the differences in apparent fracture toughness values obtained from specimens with different configurations can be better understood and taken into account.

SUMMARY OF APPENDED PUBLICATIONS

Publication 1 (Appendix 1) presents very detailed finite element analyses of standardized fracture toughness test specimens (3PB- and CT-specimen). The constraint variation along the 3-dimensional crack front has been modelled by means of small-scale yielding correction (SSYC) and J-Q approach as functions of specimen and crack dimensions and strain hardening exponent of the applied deformation hardening material model. Both methods for constraint description yielded similar type of results. The constraint characteristics of a configuration were found to be strongly related to the variations of principal stress contours around the crack tip as a function of thickness position. The size of the principal stress contour corresponding to the stress value critical with respect to cleavage fracture appeared to decrease at crack front positions closer to the free side surface of the specimen, compared to high constraint conditions at the center of the crack front. Side grooving did not decrease the constraint loss significantly. By considering the size of the principal stress contour with respect to specimen thickness, a definition for effective specimen thickness was derived, referring to the volume in which critical conditions for cleavage fracture initiation exist. Thus, the effective thickness seems to be a good parameter for ranking the specimen configurations with respect to susceptibility for cleavage fracture.

Publication 2 (Appendix 2) presents a similar type of analysis for two semielliptical surface cracks in a plate in four-point bending as Publication 1 for standardized specimens. The plate dimensions and strain hardening exponent of the deformation hardening material model were the same, while only the effect of the surface crack dimensions on the constraint characteristics were studied. The wider and deeper (i.e. larger) surface crack seemed to follow better the SSY conditions to larger deformation levels than the smaller surface crack in terms of toughness scaling models and J-Q behaviour. A comparison of the constraint characteristics between both surface cracks and a standardized three-point bend specimen with $a/W = 0.5$ was conducted. It appeared that the surface cracks loose their constraint at much lower deformation levels in terms of normalised J-integral than the standardized fracture toughness test specimen, which indicates that standardized tests produce too conservative fracture toughness estimates with respect to realistic semielliptical flaws in components. A formula for the J-integral for the surface crack was derived and a test serie with both standardized specimens and surface cracked plates was conducted to give verification to the formula. Determined brittle-to-ductile transition curves for both specimen types indicated that the transition region for the surface cracks is at lower temperature range than the transition region for the three-point bend specimens. Combined constraint and thickness correction was applied to the test results in order to obtain specimen geometry independent fracture toughness values.

Publication 3 (Appendix 3) presents empirical test results of Charpy-size impact specimens with varying precrack a/W ratios. The original, uncorrected test results showed a strong dependence on a/W ratio. The loss of constraint was attempted to correct by using T-sress, Q-parameter and small-scale yielding correction (SSYC) methods. The SSYC seemed to be most succesfull in the task, being able to give quantitative constraint correction, while T and Q served best as qualitative indexing parameters.

In Publication 4 (Appendix 4) the results of Publication 3 were presented with results of a static test serie of 4PB specimens with specimen thickness ranging from 5 to 300 mm. The apparent fracture toughness was found to increase with decreasing thickness. Both a statistical thickness correction and an effective thickness correction were applied to the test results presenting the results in a uniform way with only small scatter.

REFERENCES

Ainsworth, R. A. & O'Dowd, N. P. 1994. Constraint in the failure assessment diagram approach for fracture assessment. Proc. of the 1994 Pressure Vessels and Piping Conference, Minneapolis, MN, USA. New York: ASME. Pp. 137 - 145.

Al-Ani, A. M. & Hancock, J. W. 1991. J-dominance of short cracks in tension and bending. Journal of Mechanics and Physics of Solids, Vol. 39, No. 1, pp. 23 - 43.

Anderson, T. L. & Dodds, R. H. 1991. Specimen size requirement for fracture toughness testing in the transition region. Journal of Testing and Evaluation, JTEVA, Vol. 19, No. 2, pp. 123 - 134.

ASTM Standard E399-90. Standard test method for plane-strain fracture toughness of metallic materials. Annual Book of ASTM Standards, 1996, Vol. 3.01.

Batdorf, S. B. & Crose, J. G. 1974. A statistical theory for the fracture of brittle structures subjected to nonuniform polyaxial stresses. Journal of Applied Mechanics, Transactions of ASME, Vol. 41, June, pp. 459 - 464.

Begley, J. A. & Landes, J. D. 1972. The J integral as a fracture criterion. Fracture Toughness, Proceedings of the 1971 National Symposium on Fracture Mechanics, Part II. ASTM STP 514. Philadelphia, PA: American Society for Testing and Materials. Pp. 1 - 20.

Beremin, F. M. 1983. A local criterion for cleavage fracture of a nuclear pressure vessel steel. Metallurgical Transactions 14A, November, pp. 2277 - 2287.

Betegòn, C. & Hancock, J. W. 1991. Two-parameter charaterization of elastic-plastic crack-tip fields. Journal of Applied Mechanics, Vol. 58, No. 1, pp. 104 - 110.

Bilby, B. A., Cardew, G. E., Goldthorpe, M. R. & Howard, I. C. 1986. A finite element investigation of the effect of specimen geometry on the fields of stress and strain at the tip of stationary cracks. Size Effects in Fracture. London: Institution of Mechanical Engineers. Pp. 37 - 46.

Brocks, W. & Olschewiski, J. 1986. On J-dominance of crack-tip fields in largely yielded 3d structures. International Journal of Solids and Structures, Vol. 22, No. 7, pp. 693 - 708.

DeLorenzi, H. G. & Shih, C. F. 1983. 3-d elastic-plastic investigation of fracture parameters in side-grooved compact specimen. International Journal of Fracture, Vol. 21, pp. 195 - 220.

Dodds, R. H. 1991. Private communication.

Dodds, R. H. 1993. Unpublished research.

Dodds, R. H., Anderson, T. L. & Kirk, M. T. 1991. A framework to correlate a/W ratio effects on elastic-plastic fracture toughness (J_c). International Journal of Fracture, Vol. 48, No. 1, pp. 1 - 22.

Du, Z.-Z. & Hancock, J. W. 1991. The effect of non-singular stresses on crack-tip constraint. Journal of Mechanics and Physics of Solids, Vol. 39, No. 4, pp. 555 - 567.

Eshelby, J. D. 1956. The continuum theory of lattice defects. Solid State Physics, Advances in Research and Applications. Vol. 3. New York: Academic Press Inc. Pp. 79 - 144.

Evans, A. G. 1978. A general approach for the statistical analysis of multiaxial fracture. Journal of The American Ceramic Society, Vol. 61, July - August, pp. 302 - 308.

Faleskog, J. 1994. Crack growth in elastic-plastic materials. Dissertation. Stockholm, Sweden: Royal Institute of Technology. 20 p. + app. 148 p.

Faleskog, J., Zaremba, K., Nilsson, F. & Öberg, H. 1991. An investigation of two- and three-dimensional elasto-plastic crack growth experiments. Defect Assessment in Components - Fundamentals and Applications, ESIS EFG9. Blauel, J. G. & Schwalbe, K.-H. (Eds.). Mechanical Engineering Publications. Pp. 333 - 343.

Franco, C. & Gilles, P. 1992. Three-dimensional elastic-plastic analysis of small circumferential surface cracks in pipes subjected to bending loads. Fracture Mechanics: Twenty-Second Symposium (Volume II), Atluri, S. N., Newman, J. C., Raju, I. S. & Epstein, J. S. (Eds.). American Society for Testing and Materials. Pp. 183 - 205.

Hancock, J. W., Reuter, W. G. & Parks, D. M. 1993. Constraint and toughness parameterized by T. In: Hackett, E. M., Schwalbe, K.-H. and Dodds, R. H. (Eds.). Constraint Effects in Fracture. ASTM STP 1171. Philadelphia, PA: American Society for Testing and Materials. Pp. 21 - 40.

Harlin, G. & Willis, J. R. 1988. The influence of crack size on the ductile-brittle transition. Proceedings of the Royal Society of London, Vol. A415, pp. 197 - 226.

Hayes, D. J. 1970. Some applications of elastic-plastic analysis of fracture mechanics. Ph.D. Dissertation. London: Imperial College, University of London.

Hutchinson, J. W. 1968. Singular behaviour at the end of a tensile crack in a hardening material. Journal of Mechanics and Physics of Solids, Vol. 16, pp. 13 - 31.

Iwadate, T. & Yokobori, T. 1994. Evaluation of elastic-plastic fracture toughness testing in the transition region through Japanese interlaboratory tests. Fracture Mechanics: Twenty-Fourth Volume, ASTM STP 1207, Landes, J. D., McCabe, D. E. & Boulet, J. A. M. (Eds.). American Society for Testing and Materials. Pp. 233 - 263.

Kirk, M. T., Koppenhoefer, K. C. & Shih, C. F. 1993. Effect of constraint on specimen dimensions needed to obtain structurally relevant toughness measures. In: Hackett, E. M., Schwalbe, K.-H. and Dodds, R. H. (Eds.). Constraint Effects in Fracture. ASTM STP 1171. Philadelphia, PA: American Society for Testing and Materials. Pp. 79 - 103.

Kumar, V. & German, M. D. 1988. Nonlinear analysis of surface cracks in cylinders. Analytical, Numerical and Experimental Aspects of Three Dimensional Fracture Processes: Joint ASME/SES Applied Mechanics and Engineering Sciences Conference, Berkeley, CA, June 20 - 22, 1988. ASME AMD-Vol. 91. New York: ASME. Pp. 63 - 87.

Landes, J. D. & Begley, J. A. 1972. The effect of specimen geometry on J_{Ic}. fracture toughness. Proceedings of the 1971 National Symposium on Fracture Mechanics, Part II. ASTM STP 514. Philadelphia, PA: American Society for Testing and Materials. Pp. 24 - 39.

Larsson, S. G. & Carlsson, A. J. 1973. Influence of non-singular stress terms and specimen geometry on small-scale yielding at crack tips in elastic-plastic materials. Journal of Mechanics and Physics of Solids, Vol. 21, pp. 263 - 277.

Leevers, P. S. & Radon, J. C. 1983. Inherent stress biaxiality in various fracture specimen geometries. International Journal of Fracture, Vol. 19, pp. 311 - 325.

McMeeking, R. M. & Parks, D. M. 1979. On criteria for J-dominance of crack-tip fields in large-scale yielding. In: Landes, J. D., Begley, J. A. and Clarke. G. A. (Eds.). Elastic-Plastic Fracture. ASTM STP 668. Philadelphia, PA: American Society for Testing and Materials. Pp. 175 - 194.

Mudry, F. 1987. A local approach to cleavage fracture. Nuclear Engineering and Design, Vol. 105, pp. 65 - 76.

Nakamura, T., Shih, C. F. & Freund, L. B. 1989. Three-dimensional transient analysis of a dynamically loaded three-point bend ductile fracture specimen. Nonlinear Fracture Mechanics: Volume I - Time-Dependent Fracture, ASTM STP 995, Saxena, A., Landes, J. D. & Bassani, J. L. (Eds.), American Society for Testing and Materials. Pp. 217 - 241.

Narasimhan, R., Rosakis, A. J. & Zehnder, A. T. 1988. Three dimensional fields for a through crack in an elastic-plastic solid: numerical analysis and comparison with interferometric measurements. Analytical, Numerical and Experimental

Aspects of Three Dimensional Fracture Processes: Joint ASME/SES Applied Mechanics and Engineering Sciences Conference, Berkeley, CA, June 20 - 22, 1988. ASME AMD-Vol. 91. New York: ASME. Pp. 239 - 254.

Newman, J. C. & Raju, I. S. 1984. Stress-intensity factor equations for cracks in three-dimensional finite bodies subjected to tension and bending loads. Virginia, U.S.A: NASA. 38 p. (NASA Technical Memorandum 85793.)

O'Dowd, N. P. 1995. Applications of two parameter approaches in elastic-plastic fracture mechanics. Engineering Fracture Mechanics, Vol. 52, No. 3, pp. 445 - 465.

O'Dowd, N. P. & Shih, C. F. 1991. Family of crack-tip fields characterized by a triaxiality parameter. I. Structure of fields. Journal of Mechanics and Physics of Solids, Vol. 39, No. 8, pp. 989 - 1015.

O'Dowd, N. P. & Shih, C. F. 1992. Family of crack-tip fields characterized by a triaxiality parameter. II. Fracture applications. Journal of Mechanics and Physics of Solids, Vol. 40, No. 5, pp. 939 - 963.

O'Dowd, N. P. & Shih, C. F. 1994. Two parameter fracture mechanics: Theory and applications. In: Landes, J. D., McCabe, D. E. and Boulet, J. A. M. (Eds.) Fracture Mechanics. ASTM STP 1207. Philadelphia, PA: American Society for Testing and Materials. Pp. 21 - 47.

Parks, D. M. 1990. A surface crack reviev: elastic and elastic-plastic behaviour. Surface Crack Growth: Models, Experiments, and Structures, ASTM STP 1060, Reuter, W. G., Underwood, J. H. & Newman, J. C. Jr (Eds.). American Society for Testing and Materials. Pp. 9 - 33.

Parks, D. M. 1991. Three-dimensional aspects of HRR-dominance. In: Blauel, J. G. and Schwalbe, K.-H. (Eds.). Defect Assessment in Components - Fundamentals and Applications, ESIS/EGF9. London: Mechanical Engineering Publications. Pp. 205 - 231.

Parks, D. M. & Wang, Y.-Y. 1988. Elastic-plastic analysis of part-through surface cracks. Analytical, Numerical and Experimental Aspects of Three Dimensional Fracture Processes: Joint ASME/SES Applied Mechanics and Engineering Sciences Conference, Berkeley, CA, June 20 - 22, 1988. ASME AMD-Vol. 91. New York: ASME. Pp. 19 - 32.

Reuter, W. G., Underwood, J. H. & Newman, J. C. Jr. 1990. Overview. Surface Crack Growth: Models, Experiments, and Structures, ASTM STP 1060. Reuter, W. G., Underwood, J. H. & Newman, J. C. Jr. (Eds.). American Society for Testing and Materials. Pp. 1 - 5.

Rice, J. R. 1968. A path independent integral and the approximate analysis of strain concentration by notches and cracks. Journal of Applied Mechanics, Transactions of the ASME, June, pp. 379 - 386.

Rice, J. R. 1974. Limitations to the small scale yielding approximation for crack tip plasticity. Journal of Mechanics and Physics of Solids, Vol. 22, pp. 17 - 26.

Rice, J. R. & Rosengren, G. F. 1968. Plane strain deformation near a crack tip in a power-law hardening material. Journal of Mechanics and Physics of Solids, Vol. 16, No. 1, pp. 1 - 12.

Ritchie, R. O., Knott, J. F. & Rice, J. R. 1973. On the relationship between critical tensile stress and fracture toughness in mild steel. Journal of Mechanics and Physics of Solids, Vol. 21, pp. 395 - 410.

Santaoja, K. 1992. Some remarks upon fracture mechanics. Espoo: Technical Research Centre of Finland. 66 p. + app. 8 p. (VTT Publications 100).

Santaoja, K. 1996. Rectilinear crack growth in hyperelastic materials. Espoo: Technical Research Centre of Finland. 77 p. + app. 13 p. (VTT Publications 275).

Sham, T.-L. 1991. The determination of the elastic T-term using higher order weight functions. International Journal of Fracture, Vol. 48, pp. 81 - 102.

Shih, C. F. & German, M. D. 1981. Requirements for a one parameter characterization of crack tip fields by the HRR singularity. International Journal of Fracture, Vol. 17, No. 1, pp. 27 - 43.

Tada, H., Paris, P. & Irwin, G. 1985. The stress analysis of cracks handbook. 2nd ed. St. Louis, Missouri, USA: Paris Productions Inc. 500 p.

Theiss, T. J., Shum, D. K. M. & Rolfe, S. T. 1994. Interim results from the heavy section steel technology (HSST) shallow-crack fracture toughness program. Fracture Mechanics: Twenty-Fourth Volume, ASTM STP 1207. Landes, J. D., McCabe, D. E. & Boulet, J. A. M. (Eds.). American Society for Testing and Materials. Pp. 131 - 151.

Tvergaard, V. & Hutchinson, J. W. 1994. Effect of T-stress on mode I crack growth resistance in a ductile solid. International Journal of Solids and Structures, Vol. 31, No. 6, pp. 823 - 833.

Van Der Sluys, W. A. & Miglin, M. T. 1994. Results of MPC/JSPS cooperative testing program in the brittle-to-ductile transition region. Fracture Mechanics: Twenty-Fourth Volume, ASTM STP 1207. Landes, J. D., McCabe, D. E. & Boulet, J. A. M. (Eds.). American Society for Testing and Materials. Pp. 308 - 324.

Wallin, K. 1984. The scatter in K_{Ic}-results. Engineering Fracture Mechanics, Vol. 19, No. 6, pp. 1085 - 1093.

Wallin, K. 1985. The size effect in K_{Ic} results. Engineering Fracture Mechanics, Vol. 22, No. 1, pp. 149 - 163.

Wallin, K. 1991. Statistical modelling of fracture in the ductile-to-brittle transition region. In: Blauel, J. G. and Schwalbe, K.-H. (Eds.). Defect Assessment in Components - Fundamentals and Applications. ESIS/ ECGF9. London: Mechanical Engineering Publications. Pp. 415 - 445.

Wallin, K., Saario, T. & Törrönen, K. 1984a. Statistical model for carbide induced brittle fracture in steel. Metal Science, Vol. 18, No. 1, pp. 13 - 16.

Wallin, K., Saario, T., Törrönen, K. & Forstén, J. 1984b. Mechanism based statistical evaluation of the ASME reference fracture toughness curve. Proc. of Fifth International Conference on Pressure Vessel Technology, San Francisco, California, U.S.A., 9 - 19 September 1984. Vol. II. Materials and Manufacturing. New York: ASME. Pp. 966 - 974.

Weibull, W. 1939. The phenomenon of rupture in solids. Stockholm, Sweden: Royal Technical University. 55 p. (Ingeniörsvetenskapsakademiens handlingar nr 153).

Williams, M. L. 1957. On the stress distribution at the base of a stationary crack. Journal of Applied Mechanics, Vol. 24, March, pp. 109 - 114.

Xia, L., Wang, T. C. & Shih, C. F. 1993. Higher-order analysis of crack-tip fields in power law hardening materials. Journal of Mechanics and Physics of Solids, Vol. 41, pp. 665 - 678.

Appendices of this publication are not included in the PDF version. Please order the printed version to get the complete publication (http://www.inf.vtt.fi/pdf/publications/1997/)